FLEXURAL PROPERTIES OF HYBRIDIZED UNIDIRECTIONAL COMPOSITES REINFORCED WITH BAMBOO AND BASALT FIBERS

By

Mario Calderon Cueva

A THESIS

Submitted
to Michigan State University
in partial fulfillment of the requirements
for the degree of

Materials Science and Engineering – Master of Science

2018

ABSTRACT

FLEXURAL PROPERTIES OF HYBRIDIZED UNIDIRECTIONAL COMPOSITES REINFORCED WITH BAMBOO AND BASALT FIBERS

By

Mario Calderon Cueva

In the present work, the flexural properties of hybridized composites with bamboo and basalt as reinforcing agents in an epoxy matrix (DGEBA + mPDA) are studied. Unidirectional composites with different weight ratio content of fibers were mechanically evaluated using three-point bending tests. The peak value for flexural modulus of the hybrid composites was observed in composites with a weight ratio of 30/10 of bamboo to basalt, while composites with the highest basalt content exhibited the maximum strength. The physical and chemical properties of bamboo and basalt fibers were characterized with thermogravimetry. Bamboo fibers were processed from raw culms via ammonia freeze explosion *AFEX* and with steam explosion. The adhesion of basalt fibers (without sizing) with the matrix was investigated with single fiber fragmentation tests. Fracture surfaces of the basalt, bamboo, and hybrid composites were evaluated to assess the synergistic behavior of the combination of the bamboo and the basalt fibers in the matrix. The failure characteristics of the samples subjected to flexural load were analyzed by evaluating the morphology of the fracture surface using scanning electron microscopy. The results of this study show high values of flexural properties of bamboo/basalt fiber composites, for the production of high-quality, environmentally-benign, and sustainable materials. These properties could be optimized by the surface treatment of basalt fibers to make the matrix and these fillers more compatible. Additionally, the parameters for the AFEX treatment can be further investigated to improve the performance of bamboo as reinforcement.

ACKNOWLEDGMENTS

My deepest appreciation to my advisor, Prof. Lawrence T. Drzal, for his support from the beginning of my studies at Michigan State University. He is an inspiration for me for his knowledge, his creative mind, and for encouraging me to think always think critically. My sincere appreciation to Prof. Alex Zevalkink and Prof. Ramani Narayan for being part of my commitee. I thank them for their time and effort for rewiewing this work.

I want to thank the Composite Materials and Structures Center staff for their support throughout this process: Mike Rich, Brian Rook, Per Askeland, and Ed Drown. I am deeply grateful for their advice and their constant willingness to provide me guidance in my experimental work. Also, I would like to thank my colleages in my research group and my friends; David and Saeeda Smiadak, Erik Stitt, and Eureka Pai. They have encouraged and motivated me greatly during this process.

Finally, I want to thank my sister, my mom, and my dad -my eyes in the sky-. Their had work, honesty, and tenacity are values that I admire greatly and have been of great help in my endeavour as a researcher. My deep appreciation to my girlfriend, María Emilia, for always believing in me.

TABLE OF CONTENTS

LIST OF TABLES

LIST OF FIGURES

KEY TO ABBREVIATIONS

EPON$^{\text{TM}}$ 828	Bisphenol A diglycidyl ether (DGEBA)
mPDA	m-Phenylenediamine
TGA	Thermogravimetric analysis
SEM	Scanning electron microscopy
AFEX	Ammonia freeze explosion process
DI-water	Deionized water
SFFT	Single-fiber fragmentation test
IFSS	Interfacial shear strength
N	Number of samples
$\bar{x}$	Sample mean
SD	Standard deviation of the sample (s), given by $s = \sqrt{\frac{\sum_{i=1}^{N}(x_i - \bar{x})^2}{N-1}}$
SE	Standard error of the sample $(s_{\bar{x}})$, given by $s_{\bar{x}} = \frac{s}{\sqrt{N}}$
ROM	Rule of mixtures
LCC	Lignin-carbohydrate complex

CHAPTER 1

INTRODUCTION

Composite materials are characterized by the combination of two or more types of materials to create a material, that, if well designed, will exhibit the best features of each type. The convention is to call *composites* the macroscopic combination of different materials[34]. Although there are many different types of composite materials, there is a great interest in fiber-reinforcement of a polymeric binder (a *matrix*). Fibers possess high length to diameter ratio, and excellent stiffness and strength to density ratio. However, fibers (also called *fillers* in this context) are not useful if they are not structurally stable. For this reason, it is necessary to embed the fibers in a matrix. This type of materials are called *fibrous composites*. Fibrous composites consisting of carbon or boron fibers in low-toughness epoxies were first studied in the 1960s in the United States for their application in aerospace and defense areas[12]. Since then, many studies have been conducted to improve the mechanical properties of the matrix, strengthen the fibers, improve the adhesion between the fillers and design and create better ways to produce synthetic fibers. The most commonly used fibers are glass, comprising 95% of the reinforcement of thermosets and thermoplastics[48]. The issue with this type of synthetic fiber lies in the generation of waste for its production. For this reason, the present study presents *basalt fibers* as an alternative to glass fibers. Basalt is a vulcanic compound of several oxides that represents more than 30% of the earth's crust[15]. The production of these fibers does not require the addition of secondary products and the mechanical properties are comparable to those of glass-fibers.

Additionaly, in an effort to create more eco-friendly products, as well as a way to enhance the composite properties, *cellulosic fibers* are now being widely studied. Essentially, all natural fibers share cellulose (the structural component) and lignin (the bonding agent between cellulose) in different ratios and concentrations. Although natural fibers were already used in plastics (phenolic systems) in the beginning of the 20th century, there is a an increasing interest in the implementation of ligno-cellulosic fibers in recent decades, especially due to the imperative need to increase ductility of the composite by the addition of fibers that possess higher elongation at break. Also, the use of natural fibers is a way to tackle the environmental concern regarding the disposal of composites when they have completed their life cycle, the increasing demand of resources by the population growth and the potential economic growth of agricultural communities by the production of bio-based fibers. Although some natural fibers have been developed to have comparable properties of glass fibers, there are inherent limitations to the natural fibers, which will be discussed later in detail.

Since the ultimate goal is to produce an environmentally-friendly composite of excellent mechanical properties, the need to produce a bio-degradable matrix of comparable characteristics of the traditional polymers is still pending. A bio-degradable polymer is a system that is fully degraded by aerobic (CO_2), anaerobic (methane) processes, or by micro-organisms[21]. It is worth mentioning that not all bio-based polymers are biodegradable, and not all biodegradable polymers are bio-based.

Although the present study investigates the flexural properties of bamboo fibers combined with basalt fibers as fillers in a non-biodegrabale epoxy matrix, it should serve as a basis to demonstrate the positive effect of combining these two types of fibers towards a sustainable final product that could be potentially implemented on a large scale.

1.1 Objectives

The goal of the present work is to fabricate hybrid composites that are environmentally benign while meeting the quality standards for structural and semistructural applications. This study aims to identify the potential of combining natural fibers with synthetic fibers, referred to as *hybridization* of composites, to achieve a synergistic effect in flexural properties in an epoxy matrix. For this purpose, a series of tests were conducted to characterize the bamboo and the basalt fibers as individual entities, as well as their behavior in the composites.

1.2 Materials

1.2.1 Matrix

The matrix selected for this work was an epoxy resin of DGEBA with 14.5 parts per hundred of resin (*phr*) of mPDA. The selection of this thermosetting system was due to its high mechanical properties, as well as the well-studied adhesion behavior with many fillers. All composites for flexural tests were prepared with the same composition of the matrix under the same conditions, and with the same commercial product (EPON 828 - from Miller Stephenson Company and mPDA - from Sigma Aldrich). The matrix was cured at 75ºC for 2 hours in a convection oven, followed by a post curing of 2 hours at 125ºC. The flexural modulus and strength reported for this polymeric matrix are 2.9GPa and 95MPa, respectively[41]. This epoxy system has an elongation at break of around 5% and a density of $1.2\frac{\mathrm{g}}{\mathrm{cm}^3}$[25].

1.2.2 Fibers

1.2.2.1 Bamboo

The bamboo fibers were received as untreated sections of the culm of 30cm long, with an outer diameter of around 10cm and a inner diameter of approximately 8cm. The compoany Resource Fiber LLC, based in Alabama, USA, provided the fibers. The species of the provided bamboo culms are Phyllostachys edulis, also known as *Moso*. It was not possible to determine the age of the bamboo, since the dimensions of the culm, as well as other features depend on the growing conditions, such as the humidity of the region, the amount of rain the culm received, the sun exposure, and the soil.[53]. There is an inherent variability of the mechanical and physical properties for the untreated bamboo fibers. These characteristics depend on many factors, such as the age of the specimen, the height, the position of the fiber with respect to radius of the bamboo, among others. Consequently, the physical and mechanical characteristics of the fibers reported in the literature show a range of values[17][16]. In the present work, the term *bamboo fiber* is used interchangeably with *fiber-bundle*. For bamboo, a fiber-bundle is composed by hundreds of individual fibers, that cannot be separated by the processes used in this study. All bamboo specimens tested in this work are fiber-bundles. When it is important to make a differentiation between fibers and fiber-bundles, the fiber would be refered as *individual fiber*. This is the case of section 3.1.

- Density:$0.8 - 1.1\frac{\mathrm{g}}{\mathrm{cm}^3}$
- Elongation at break $5 - 10.2\%$
- Flexural strength $230 - 388$MPa
- Flexural modulus $11 - 15$GPa

1.2.2.2 Basalt

Basalt fibers are a product of processing . Basalt is dark, fine-grained, compact assembly of different compounds, such as magnesium-silicate and iron-silicate, and a low content of silica *basalt rock*. Although this vulcanic rock is dark, the basalt fibers were brown gold in color. After the curing process of the composites, the basalt fibers adopted a black color again. For the present study, basalt fibers were provided by MAFIC Basalt (North Carolina, USA) as assembled-roving, continuous fiber toes with a nominal fiber diameter of 13μm were not sized in any way, and the key sizing element is reported as DI-water[42]. The following properties are reported by MAFIC[42]:

- Density:$2.63\frac{\mathrm{g}}{\mathrm{cm}^3}$
- Elongation at break 3.5%
- Tensile strength 3100MPa
- Tensile modulus $88 - 92$GPa
- Moisture content $< 0.1\%$

1.3 Overview of experiments

The following experiments were conducted in the present study in order to characterize the physico-chemical of the fibers, the neat epoxy, and the fabricated composites.

1.3.1 Mechanical tests

- Three-point bending test in compliance with ASTM 790 for all composites for the calculation of flexural modulus and strength.
- Single fiber fragmentation test on basalt fibers in epoxy matrix for the evaluation of the adhesion between the fibers and the epoxy.
- Static-load three point bending test in DMA apparatus for single fiber test on AFEX-treated bamboo.

1.3.2 Physico-chemical analysis

- TGA on basalt and AFEX-treated fibers to determine the degradation temperatures of each fibers as well as the water uptake. This test was also conducted to make an initial assessment of the properties of hemicellulose, cellulose, and lignin for the AFEX-treated bamboo fibers.
- Density measurements of basalt and AFEX-treated fibers with pycnometer. The density of bamboo specimens were measured before and after drying to determine the water absorption of the fibers.
- Density measurements of basalt composites to confirm weight fraction.

1.3.3 Morphological analysis

- SEM on fracture surface for all flexural samples after testing to determine the failure mechanisms experienced by the composites.

- Transmission optical microscopy for basalt and bamboo composites to evaluate distribution and void content.
- SEM on single bamboo fiber-bundles (mechanically and AFEX treated) to identify surface roughness, and cell types present. Moreover, this test provided confirmation that the fiber-bundles were not damaged by the extracting and handling.
- ImageJ digital image processing to evaluate density of bamboo composites and make an estimation of the volume fraction.

CHAPTER 2

MATRIX CHARACTERIZATION

2.1 Introduction

The main purposes of a matrix (sometimes called *resin binder*) in a composite are to make the composite rigid and to transfer the stresses to the fibers[45]. Hence, the adequate selection of the polymer is crucial for the performance of the composite. The chosen polymer for the matrix of the present study is a thermosetting epoxy resin consisting of Bisphenol A diglycidyl ether (DGEBA) with m-Phenylenediamine (m-PDA) in a weight ratio of

$$\frac{\text{DGEBA}}{\text{mPDA}} = \frac{100g}{14.5g} \tag{2.1}$$

Thermoset systems are commonly used because they present several advantages:

- Low melt viscosity,
- Low temperatures of processing, and
- Lower cost (compared to thermoplastic resins)

Furthermore, epoxy resins are widely implemented in the composite fabrication due to their mechanical properties (even at humid and hot ambients), chemical resistance, and processability[31]. More importantly, these materials show good adhesion to several fibers.

2.2 Epoxy resins

The prefix *Epoxy* refers to compounds that contain oxygen (bonded to two other atoms in some way) as *bridge*. Epoxies are polymers formed by the *epoxide* functional group. An epoxide is a cyclic ether with a three-membered ring. The fundamental structure contains an oxygen atom bonded with two carbon atoms of a hydrocarbon . Due to the strain of the three-membered ring, this epoxide is very reactive compared to an acyclic ether[67]. The most common epoxy resin is DGEBA (see fig. 2.1), which is a polymer formed by the reaction of epichlorohydrin (1-Chloro-2,3-epoxypropane) and bisphenol A (2,2-Bis(4-hydroxyphenyl)propane). The formation of DGEBA is a two-step reaction, starting with a reaction of epichlorohydrin with an active-hydrogen compound, followed by the dehydrohalogenation with a base (usually Sodium of Potassium)[45].

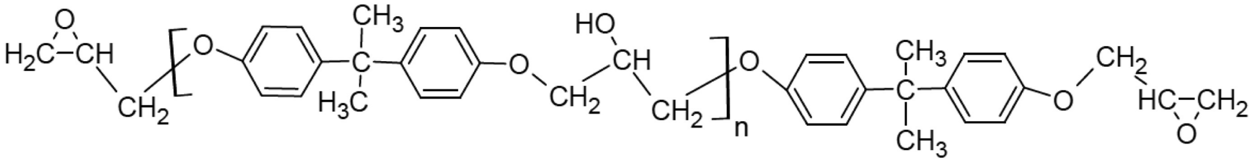

Figure 2.1 DGEBA molecule[19].

2.3 Curing agents

Curing agents can be classified into three major categories for epoxy resins (based on the functional groups): amine, acid anhydride, and acids. In the amine category, the aliphatic amine cures the resin at room temperature, while aromatic amines react very slowly at room temperature and, therefore, need higher temperatures to fully cure the epoxy[5].

The selection of the curing agent for the polymeric matrix not only affects the physical properties of the cured epoxy, but other properties such as the curing rate and cure exotherm. The curing agent selected for the present study was m-PDA (m-Phenylenediamine). Aromatic amines are chemical compounds that posses one or more planar rings of atoms bonded covalently. These bonds are of two different kinds. Amines derive from ammonia[9]. Although m-PDA has higher mechanical properties when combined with DGEBA, it also possesses health concerns.[49]. Curing with amine is accomplished by the reaction of the epoxite functional groups with the primary and secondary amines.

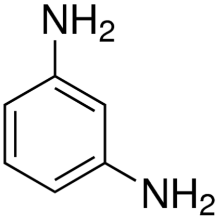

Figure 2.2 m-PDA molecule[59].

2.4 Curing process of epoxies

During the curing process, the resin experiences changes in its physical and chemical properties: The *linear polymerization* occurs, which is the formation of long chains (polymers) of covalently-bonded structures (monomers). Also, *cross-linking* takes place, which is the formation of branched structures due to bonding of the polymers formed at certain intervals. This process causes the formation of a network structure. When the polymer is cooled down after the curing process, the network structure remains because of the van-der-Waals forces that the polymers experience. Additionally, the physical properties of the resin are changed with curing, namely the viscosity and the temperature of the system[5].

2.5 Curing of epoxy resins with m-PDA

In order to achieve the desired properties, the stoichiometry of the epoxy resin with the curing agent is crucial. Therefore, the *phr* (parts per hundred of resin) of the hardener has to be calculated. Phr is defined as the ratio of the weight of resin (in grams) that contains one equivalent of epoxy (Epoxy equivalent weight - EEW) and the amine hydrogen equivalent weight (AHEW). For the EPON 828™it has been reported that the EEW of the DGEBA molecule lies between 185-195[18], while the AHEW can be calculated by the molecular weight of m-PDA $\left(108\frac{\mathrm{g}}{\mathrm{mol}}\right)$ divided by the number of active hydrogen atoms in the amine functional group. With these values AHEW = 27 and, therefore,

$$\mathrm{phr} = \frac{\mathrm{EEW}}{\mathrm{AHEW}} = 14.5[\mathrm{g}] \tag{2.2}$$

It has been reported that a system of phr = 14.5 for m-PDA with DGEBA yields the smallest heterogeneities ($\approx$ 20nm in diameter) and also the lowest occurrence. This same study shows that a heterogeneity in this polymer is a measure of a higher cross-linking density in region of lower cross-linking degree[24].

2.5.1 Curing cycle

For the present study, all polymers were cured in the same way. A beaker containing the DGEBA (EPON-828™) and another containing the m-PDA flakes (from Sigma-Aldrich) were placed at an oven at 75ºC for one hour. Subsequently, the plastic beaker with DGEBA was pured into the m-PDA container and vigorously mixed. The mixture was then placed in a vacuum oven with an internal temperature of 75ºC and degassed. The degassing process removes the air bubbles trapped in the liquid resin and also promotes the mixing of m-PDA with DGEBA. After three minutes to five minutes, the beaker is removed from the vacuum oven and put in a convection oven (already at a temperature of 75ºC). At this point, the curing takes place. The resin is held in the oven at 75ºC for two hours, upon completion, the temperature is increased to 125ºC. This step is called *post-curing*. It has been shown that the density of cross-linking dramatically increases in epoxy systems during the post-curing process and the glass transition temperature also reaches higher values[26]. When the post-curing process has ended, the oven is turned off with the resin inside until the temperature reaches 25ºC.

CHAPTER 3

FIBER CHARACTERIZATION

The quality of the fibers is a crucial parameter for the performance of the composite. Parameters such as the cristallinity, surface morphology, defect concentration, temperature degradation, and pre-treatment derive in the overall performance of the composite. The present chapter aims to characterize the physical and mechanical properties of bamboo and basalt fibers to predict and improve their behavior in the composite. Some bamboo fibers were treated via AFEX and others were extracted in a combination of steam and rolling-milling.

3.1 Bamboo fiber characteristics

3.1.1 Introduction

Bamboo belongs to the grass family of Poaceae and the subfamily of Bambusoidaeae. It represents a major economic commodity in several regions of the planet, such as India and China. Furthermore, these countries present a very large area of plantations. In the American continent, bamboo is found from Chile to Mexico (neotropical woody bamboo), while the United States shows presence of north-temperate woody bamboo. This type of bamboo is also found in continental Africa, Madagascar and Southeast Asia[69].

3.1.2 Bamboo constituents

Bamboo has three important constituents that are responsible for its features. Around 90% of the mass of bamboo is holocellulose (hemicellulose and cellulose) and lignin. Cellulose varies between 40% and 60%[2] depending on the species, age, and segment of the bamboo. α-cellulose is the type of cellulose present in bamboo and it is has the highest degree of polymerization. This type of cellulose has linear chains of β-1-4-linked glucose. Hemicelluose in bamboo is a xylan with other components (uronic acid, arabinose, xylose) in a disordered way[70]. Holocellulose has repeating subunits which promote hydrolysis. The third major component of bamboo is lignin, which is a disordered polymer composed of phenylpropanoid sub-units. These sub-units are not repeating, making hydrolisis difficult to be conducted.

3.1.3 Bamboo structure

Bamboo can be considered as a composite material, where the cellulose-microfibrils are embedded in a hemicellulose-lignin matrix, called the *lignin-carbohydrate complex* (LCC). Figure 3.1(a) shows a cross-section of a bamboo culm. The subsequent images ((b)-(e)) present in greater magnification the hierarchical structure of the ligno-cellulosic structure.

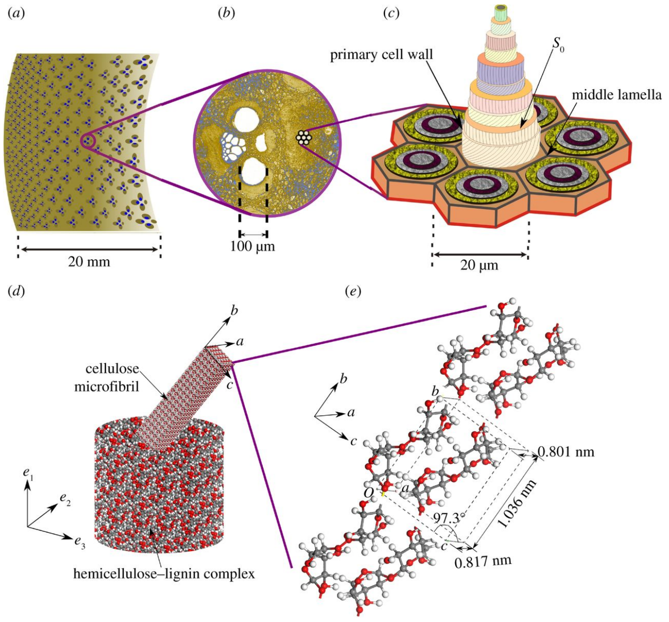

Figure 3.1 Hierarchical structure of bamboo[44]

As mentioned in chapter 1, the present study used *fiber bundles* retrieved from the trunk of bamboo of the *Moso* species. The trunk of bamboo, called the *culm*, is a hollow cylinder divided by sections that go in transversal direction with respect to the culm. These transverse sections are called the *nodes*, and they separate the *internodes*. The convention is to ennumerate the internodes starting from the ground. For the present work, the fiber bundles were extracted from the internodes at different heights of the bamboo. These fiber bundles are primarily oriented in the axial direction of the bamboo. Fiber bundles, knwon also as *sclerenchyma* cells, are composed of hundreds of individual cellulose fibers in a LCC complex. These fiber bundles have a diameter of a few hundreds micrometers. They surround the hollow vessels, namely the *protoxylem*, *phloem*, and *metaxylem*. These vessels transport water, nutrients, and products of photosynthesis between the roots and the leaves. Fiber bundles, together with these vessels form a structure called a *vascular bundle* - see figure 3.3-. The presence of vascular bundles increases from the inner to the outer side of the culm, suggesting that the structural properties of bamboo are given by fiber bundles[17]. The amount of fiber bundles varies also as a function of the height of bamboo, such that, for Moso, the fiber bundle density increases towards the internodes away from the ground. layer of the culm has a greater density of individual fibers compared to the inner side[43]. Moreover, the distribution of foam-like cells, known as *parenchyma* cells modify the density and the strength of the fibers. These type of cells can be observed in figure 3.2, on the surface of the fiber bundle. Parenchyma cells are present in bamboo along the fiber bundles, as displayed on the bottom right region of figure 3.1, and their main purpose is the transport of nutrients. It is desireable to remove them to increase the modulus of the composite. However, this can not always be done.

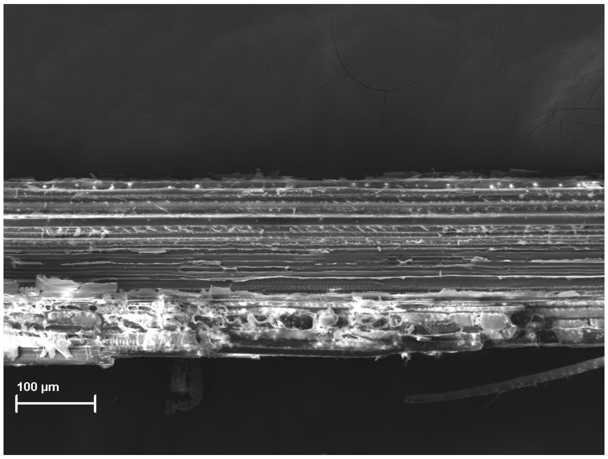

Figure 3.2 Fiber bundle micrograph (SEM) of mechanically treated bamboo. Note presence of parenchyma cells and residues of lignin/hemicellulose.

Figure 3.3 displays the *vascular bundle*, consisting of fiber bundles for the structural stability of bamboo, parenchyma cells for the transport of water and nutrients (in the radial direction), as well as the phloem and the xylem for the same purpose in the vertical directions.

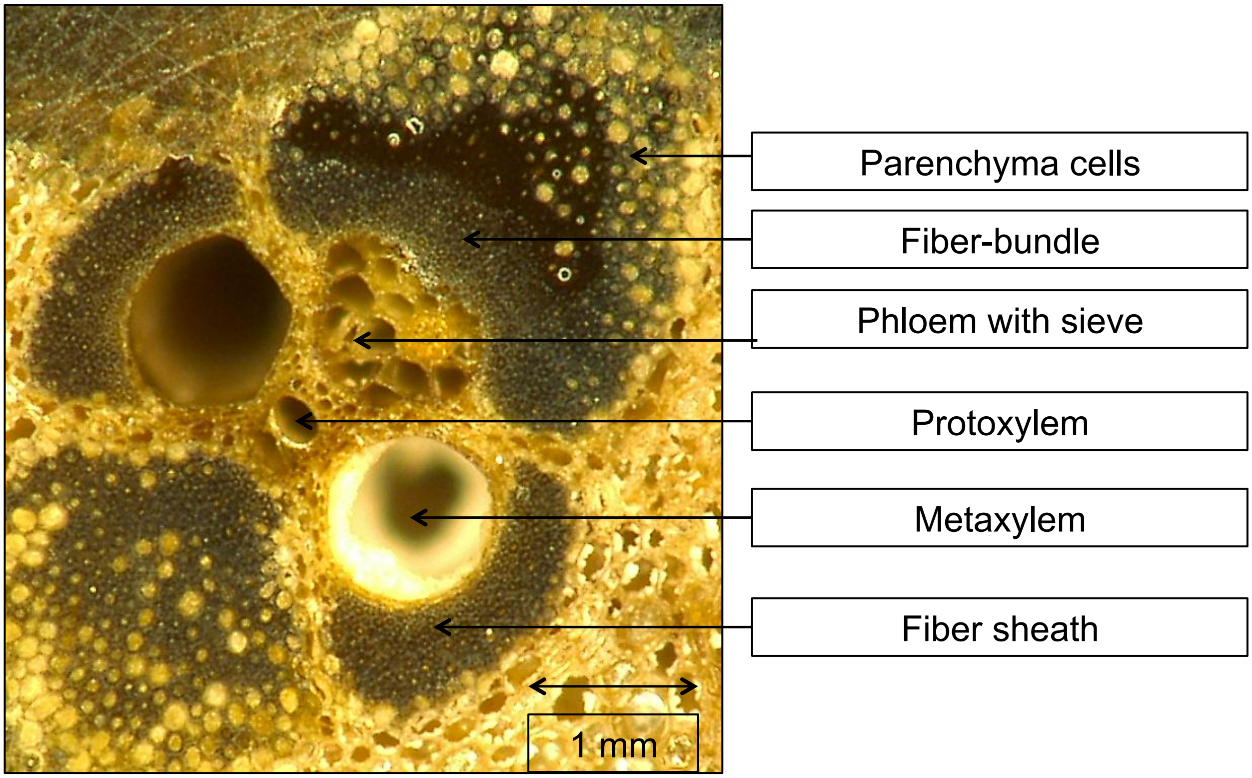

Figure 3.3 Vascular bundle of a bamboo culm. Image taken with an optical microscope.This image corresponds to the schematic figure 3.1(b)

One important aspect of the presence of the hollow regions surrounded by fibers is that it reduces the weight of the composite considerably. If figure 3.3 is further magnified, the so-called *lamellae* are observed. A lamella is a pectin compound that holds cells together. This type of structure is characterized by a concentric arrangement of cellulosic microfibrils oriented at different angles with respect to the axial direction of the fiber bundle. This microstructure is displayed in figure 3.1(c). It is proposed that thicker lamellae have microfibrils oriented close to 0º while thin lamellae exhibit a 90º angle with respect to the axial direction of the fiber[?]. In the same figure, the S_0 denotes the transition layer from the *middle lamella* to the *lumen*. The middle lamella is the lignin rich region that bonds individual fibers together in bamboo. Lumen is an aqueous phase that plays an important role in photosynthesis. The arrow in 3.4 shows the lumen of a particular individual fiber, while the circled area shows an individual fiber.

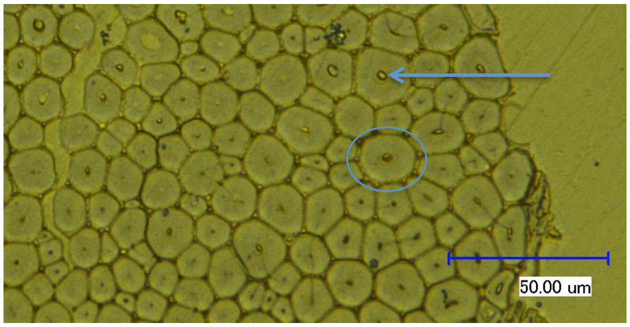

Figure 3.4 Micrograph of cross-section of bamboo fiber bundle embedded in a polymer, composed of closely packed fibers. Arrow shows lumen. Circle displays a single fiber of approx. 20μm[44]

Moreover, the differences in the sizes of the perimeter of the individual fibers in a fiber bundle are believed to be responsible for the excellent strength of bamboo[70].

Going to higher magnifications -see figure 3.1(d)- each individual fiber is composed by a single-crystal cellulosic structure, known as the *microfibril*. Each microfibril is embedded in a LCC. Every microfibril is, in turn, built of cellulose nanofibers. They are believed to be between 3 and 5 nm in diameter[50].

3.1.4 Bamboo fiber harvesting techniques

The subject of how to harvest fibers is of great importance. Its primary objective is to achieve good mechanical properties and to promote the adhesion of the fibers to the matrix.

There have been several studies regarding different techniques to retrieve fiber bundles. The most important processes for this goal are a combination of chemical and mechanical steps to separate the fiber bundles from other constituents. The most common process is the sodium hydroxide treatment (NaOH), in which bamboo strips are placed in a NaOH solution of 1.5N, where N is the *normality* (the number of OH^- ions per 1 liter of solution). The bamboo samples are kept at 70ºC for several hours and then rolling-milled for several times with a progressive increase in the pressure applied[66].

Another widely-implemented method, especially for the pulp extraction industry, is the so-called *steam explosion*. This physicochemical technique relies on the repeated pressure release of a sealed container with water. The main advantages are the low-energy consumption involved, as well as the small amount of waste produced. Additionally, the effectiveness of the production of good-quality fibers is based on the removal of lignin[58].

3.1.4.1 Mechanical extraction method

In the present study, two types of fiber extraction methods were implemented. In the first one, raw bamboo culms of an external diameter of 10cm -without removing the bark- were placed in a pressure chamber. 0.75L of DI-water were placed in the vessel. It is important to note that the bamboo samples were not fully immersed in this volume of water. The pressure vessel was then sealed. The vessel was heated with an electric-resistance oven. Then, the temperature was increased to 150ºC at a rate of 42ºC/h.The temperature of the vessel was electronically controlled with a K-type thermocouple. Since the vessel wall has a thickness of 2cm, the rate was very low. The temperature was kept at 150ºC for two hours. Finally, the heater was switched off and the system was allowed to cool down naturally until the temperature reached 90ºC. At that point, the release-valve was opened and the vessel was allowed to cool down to 30ºC. Then, the bamboo samples were taken out and manually split in segments of approximately 1cm in width. The next step was to pass the strips of bamboo through a manual rolling-mill (W Durston LTD, UK) three times. Then, the gap between the wheels was reduced by 0.5 mm. When the sample presented considerable resistance (by considering the force applied to the shaft) the gap was only decreased by 0.25 mm. When the strips showed signs of damage on the surface, the roll-milling was stopped. At this point the fiber-bundles were easily separated by hand. The bark of the samples was removed because it does not contribute to the desired mechanical properties of the fibers in the composite. The bamboo strips were placed in a convection oven at 80ºC for three hours to remove the water absorbed. In order to determine the time required to dry the bamboo the weight loss was monitored every hour. This test yielded the following results:

Table 3.1 Drying of bamboo samples after pressure-chamber treatment

Weight loss (%)	**Time (h)**
13.7	1
3.1	2
<1	3

3.1.4.2 AFEX extraction method

AFEX (Ammonia freeze explosion) treatment is a process in which the raw bamboo culms (without bark) are soaked in liquid ammonia at 50ºC for approximately 15 minutes at a pressure of 15 atm ($\approx$ 1.5 MPa). The pressure is reduced abruptly, causing a disruption of the fibrous structure of bamboo due to the violent flash of ammonia[30]. Furthermore, mechanical pressure with steam can be detrimental to the desired properties.[30][11].

AFEX treatment was originally devised as a way to process cellulosic material for the hydrolisis for feedstock purposes. The reason for this technology was that cellulose, although very abundant in plants, is surrounded by lignin and hemicellulose. These two components are not easily hydrolized. The AFEX treatment provides an effective way to access cellulose for hydrolisis. With this argument, the present work investigated the feasibility of AFEX-treatment as a way to produce high quality fibers of bamboo. In order to understand the physical changes that this treatment produced to the fiber bundles, a thermogravimetric analysis was conducted. Although the results of the AFEX-treated specimens vary strongly depending on the parameters of the reaction (temperature, pH, concentration), the result should be focused on the effectiveness of this treatment for fiber harvesting with a small reduction of cristallinity. The degree of cristallinity is an indication of the fiber strength and modulus. Some studies have shown that AFEX treatment reduces cristallinity by less than 3%[57].

3.1.5 Experiments conducted on AFEX-treated fibers

3.1.5.1 SEM images

In order to observe the morphology of the fiber after the AFEX treatment, single fiber bundles were coated with a 100nm-layer of platinum and observed in the SEM (EVO Model, ZEISS-Germany). The samples revealed to possess a high surface roughness, and some segments displayed parenchyma cells (see figure 3.5).

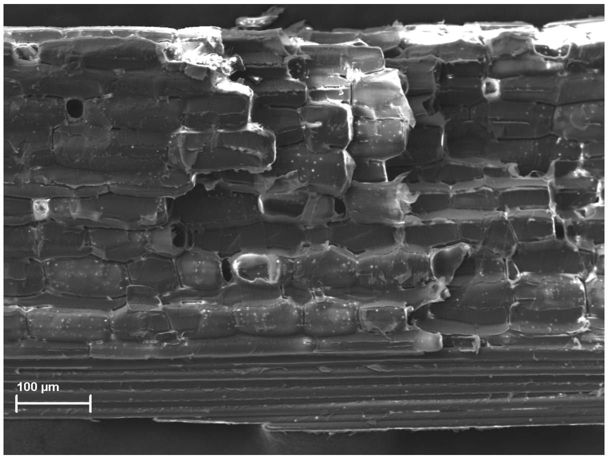

Figure 3.5 SEM image of region of a bamboo fiber-bundle showing parenchyma cells. Fiber treated with AFEX method.

3.1.5.2 TGA tests

The first test conducted to evaluate the fiber properties was a thermogravimetric analysis (TGA) of the fibers in a nitrogen atmosphere. The weight of the sample was 30.23mg. The fibers were chopped so that the could fit inside the alumina container. In order to avoid noise in the signal, the fibers were slightly pressed to create a more compact structure. The results are shown in figure 3.6. The apparatus (Q500, TA Instruments) was set to a ramp of 25ºC/min from room temperature to 500ºC since natural fibers are expected to degrade in this temperature range. This was confirmed as can be seen in the figure. From this figure, it is possible to observe that there is a multiple step process of weight loss. Moreover, there is some water desorbed[71] (see small peak at around 100ºC in the left plot of figure 3.6). Lignocellulosic materials can be characterized in their thermal behavior by the zones they degrade[60]: the hemicelluloses region (245ºC–290ºC), the cellulose region (290ºC–350ºC), and the lignin region (350ºC–500ºC), . Figure 3.6 shows that the AFEX treated samples analyzed in this work possess a high concentration of cellulose (see peak at 302ºC). Furthermore, the presence of hemicellulose is also high (peak at 280ºC). The region of lignin degradation shows two peaks of a slow degradation. The reason for the appearance of several peaks is because of the presence of different molecules present in lignin.

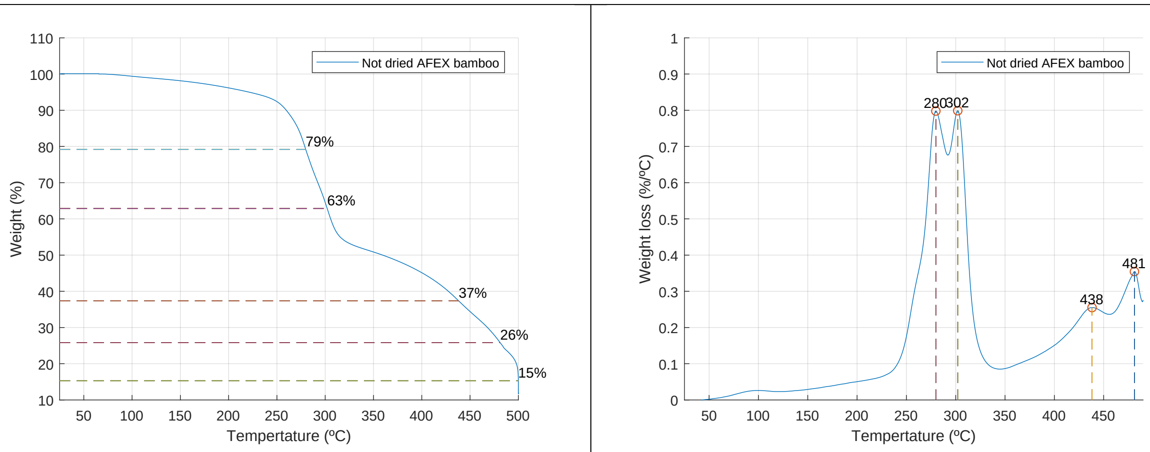

Weight loss (%) vs. temperature (ºC)

Differential weight loss (%/ºC)
vs. temperature (ºC)

Figure 3.6 Thermogravimetric analysis on AFEX-treated fibers

After this test, the effect of drying the sample was studied. A sample of 18.76mg of fibers were dried in a convection oven for two hours. Upon completion of this step, they were placed in the apparatus under the same conditions as for the undried fibers. The results of this experiment presented in figure 3.7.

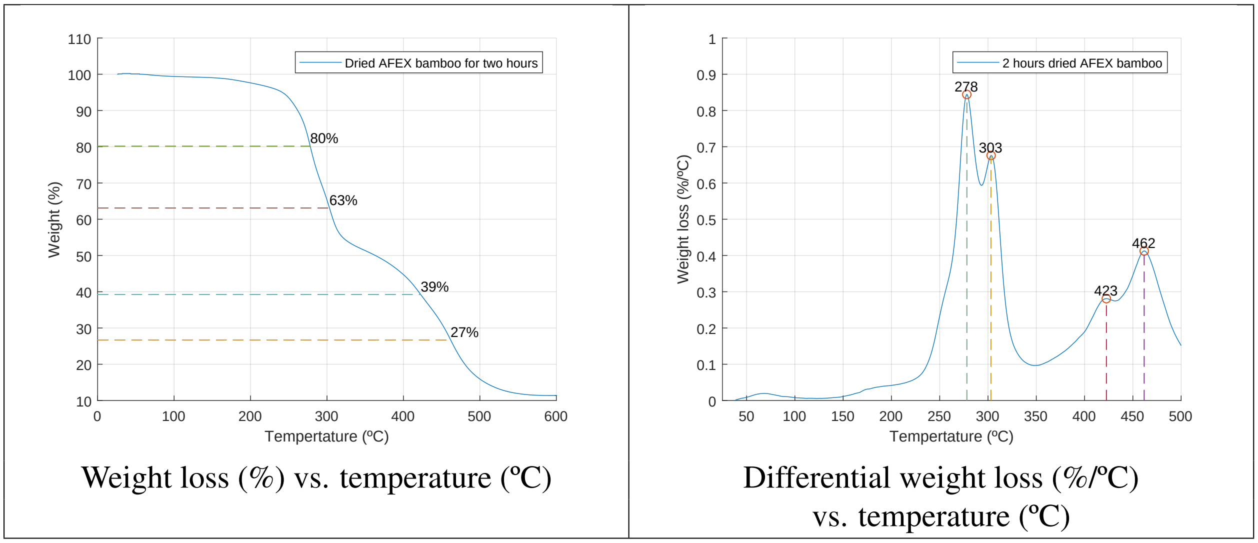

Weight loss (%) vs. temperature (ºC)

Differential weight loss (%/ºC) vs. temperature (ºC)

Figure 3.7 Thermogravimetric analysis on AFEX-treated fibers after drying for 2 hours at 80ºC

The results of this test are quite interesting from point of view of the effect of temperature on the fibers. The widths and locations of the peaks remain very similar as for the case of the undried test. However, there is a substantial reduction of the height of the cellulose peak which could mean that the drying process has enabled the access to hemicellulose sites. This could be a potential indication that the AFEX treatment can have a positive effect on the quality of the fibers.

Some studies suggest that it is not desired to remove high amounts of hemicellulose because the cellulose nano-crystals are embedded in a lignin and hemicellulose complex. If the hemicellulose is removed, the cellulose would not be able to carry the load applied because the bond-strength would be considerably reduced[57].

Density measurements To further study the behavior of the AFEX-treated fibers, density measurements in a pycnometer were performed. Samples of 2g-3g were placed in the apparatus and 10 measurements for every specimen were conducted. The following table shows the results of this experiments.

Table 3.2 Density measurements for bamboo samples

Sample characteristics	**Density** $\left(\frac{\text{g}}{\text{cm}^3}\right)$	**Standard deviation** $\left(\frac{\text{g}}{\text{cm}^3}\right)$
AFEX culm dried for 2 hours at 80ºC	1.1355	±0.0007
AFEX fibers dry 2 hours at 80ºC	1.1595	±0.0013
AFEX fibers dry 1 hour at 80ºC	1.1874	±0.0013
AFEX fibers not dried	1.2025	±0.0013

3.1.5.3 Flexural properties of single fiber bundles

The mechanical and physical properties of bamboo fiber bundles depend on many factors (e.g species, age, region, etc.)[3] [32]. In a first attempt to reduce the discrepancies in the reported flexural properties in the literature, single fiber bundles were analyzed via three-point bending tests. The fiber bundles were extracted via the mechanical process explained previously. Each fiber bundle was cut at a length of 10 mm and the diameter was measured every 2 mm under an optical transmission microscope (Keyence Corp. of America, Torrance, CA, USA). Before the test, the fibers were dried in a convection oven at 80ºC for four hours to remove the adsorbed water and other volatiles. The three-point bending test was performed in a dynamic mechanical analyzer (DMA Q800-TA Instruments, New Castle, DE, USA) under static load, with a span (L) of 5mm. The cross-section of the fiber-bundles was assumed to be circular. This assumption yields a moment of inertia about bending axis I:

$$I = \frac{\pi}{64} d^4 \tag{3.1}$$

where d is the mean diameter of the fiber bundle. The measured values that were found to be outside the interquartile range were excluded. The elastic modulus and strength of the specimens were calculated by using the equation for pure flexure where the load is applied in the midpoint of the two supports. For the elastic modulus, the equation is

$$E = \frac{mL^3}{48\Delta I} \tag{3.2}$$

where Δ is the deflection of the specimen in the midpoint between the two supports, and m is found by computing the slope of the force (N) vs. displacement (mm) in the linear region of the plot. The strength of the fiber was calculated using the equation

$$\sigma = \frac{PL}{4Z} \tag{3.3}$$

where P is the applied static force, and Z the section modulus. For the case of a circular cross-section

$$Z = \frac{\pi}{32} d^3 \tag{3.4}$$

Results The three following figures show the results of these calculations:

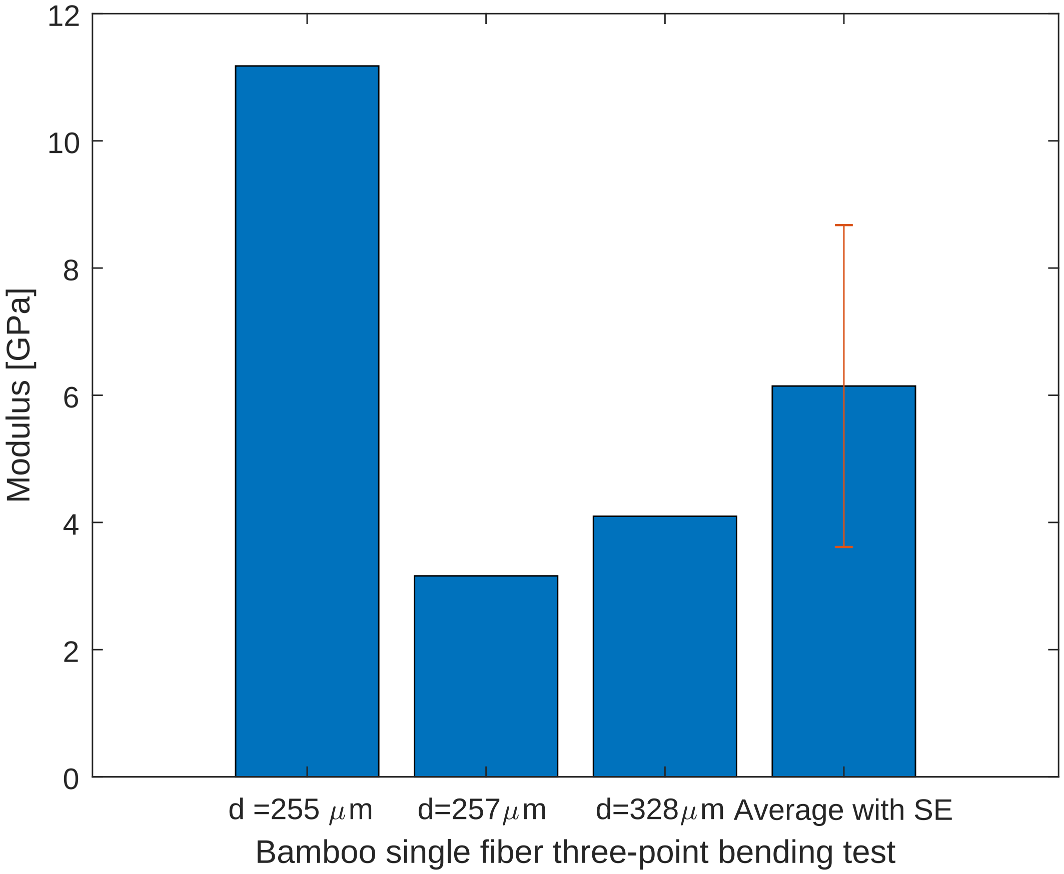

Figure 3.8 Strength of bamboo fibers, extracted with pressurized water and rolling-milled. Note significant change between the different samples

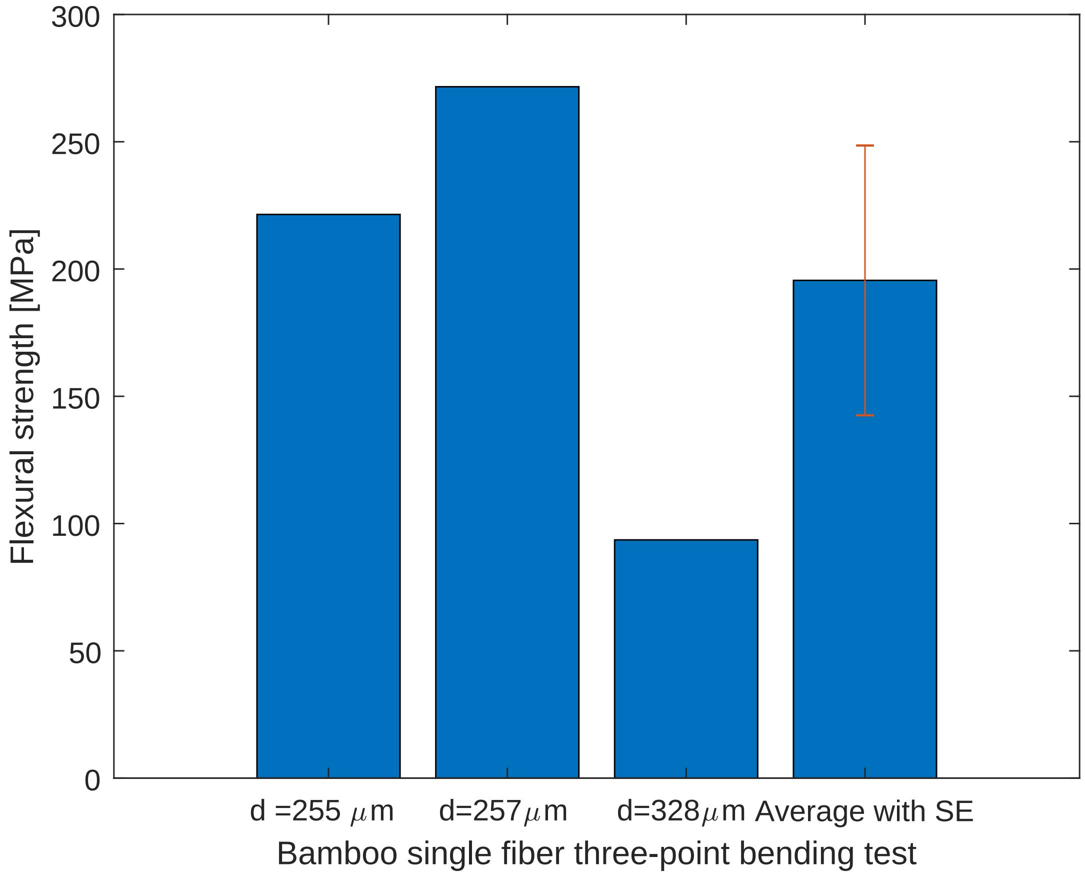

Figure 3.9 Elastic modulus of bamboo fibers, extracted with pressurized water and rolling-milled. High spread of data

As it is evident from the spread in the values for modulus and strength obtained in this test, single fiber bundle flexural tests do not give representative values for the behavior of the fibers. These values cannot be traced back to the diameter of the fiber bundle. Therefore, the approach of using a large amount of fibers (by fabricating composites) was adopted.

3.2 Basalt fiber characteristics

3.2.1 Introduction

The need to find alternatives to synthetic glass and carbon fibers with similar properties has lead to the study of basalt fibers. These fibers present a series of desired properties such as high elastic modulus, ultimate strength, stiffness, and flexibility. Perhaps the most attractive trait of these vulcanic fibers in industrial application lies in the cost advantage in specific strength and specific modulus when compared to other fibers used in composites[10]. A crucial trait for the implementation of basalt fibers lies in the lack of sizing agents for the fabrication (as opposed to glass fibers), which make this process more environmentally friendly[61]. Additionally, basalt fibers are easier to recycle, can be implemented in harsh environments and also resist higher temperatures[33].

3.2.2 Basalt structure and constituents

Basalt composition:

Table 3.3 Composition of basalt fibers

Compound	**Composition (%)**	
	A[a]	B[b]
SiO_2	52.8	51.6-57.5
Al_2O_3	17.5	16.9-18.2
Fe_2O_3	10.3	4.0-9.5
MgO	4.63	1.3-3.7
CaO	8.59	5.2-7.8
Na_2O	3.34	2.5-6.4
K_2O	1.46	0.8-4.5
TiO_2	1.38	-

[a]: taken from Jamshaid et al.[46], [b]: taken from Militky et al.[33]

3.2.3 Basalt fiber production

Compared to glass-fibers, the fabrication process of basalt fibers does not require an independent addition of other elements. Furthermore, the generation of these fibers does not yield secondary

Table 3.4 Physical and mechanical properties of basalt [a]

Properties		**Basalt filaments**
Thermal	Max. application Temperature (ºC)	980
	Sustained application temperature (ºC)	820
	Melting temperature (ºC)	1450
Physical	Density $\left(\frac{\mathrm{g}}{\mathrm{cm}^3}\right)$	2.75
	Filament diameter (mm)	9-23
	Humidity absorption (65% RAH)	0.1
Mechanical	Tensile strength (MPa)	4840
	Elastic modulus (GPa)	89
	Elongation at break (%)	3.15

[a]: Adapted from[40]

products like glass-fiber production, which is another advantage of basalt vs. glass.

There are several methods for the fabrication of basalt fibers. Since basalt fibers used in this study were provided as continuous fiber-toes, the process of fabrication of these types of filaments will be discussed.

There are two main processes for the fiberization of basalt: the melt-blowing and the centrifugal-multiroll system). In both technologies, basalt rocks are washed, crushed and melted in a container at 1450ºC[14]. The melted lava is then fed to a series of rolls. In the melt-blowing technique (also called the *Junkers method*, see figure 3.10), the melted lava is poured onto an accelerator cylinder (while air is blown towards the melted basalt). The lava then passes through the gap between two spinning cylinders roatating in opposing directions (fiberization cylinders). This process yields fibers resulting in a diameter of $6 - 10\ \mu$m.

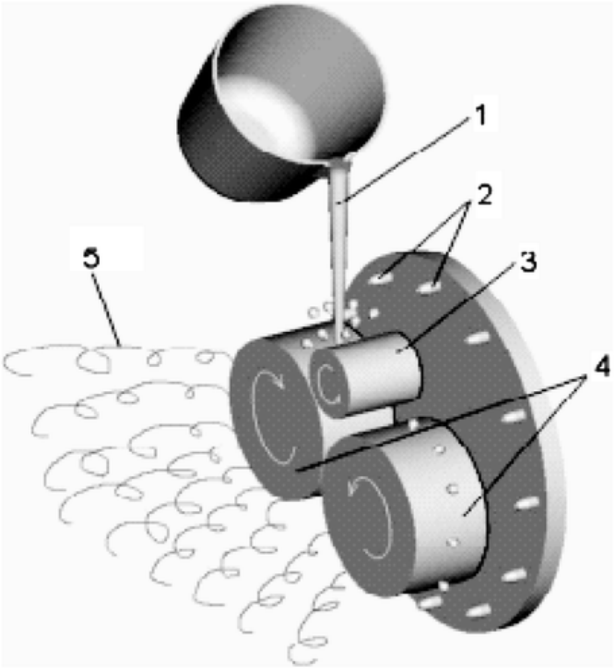

Figure 3.10 Junkers method for continuous fibers. Image taken from[33].

In figure 3.10, the numbers represent the most important components of this process.

1 : Melted lava poured to the wheels

2 : Nozzles to blow air to cool down the lava

3 : Accelerating cylinder to feed basalt into the next wheels

4 : Fiberization cylinder, rotating in opposite directions

5 : Basalt fibers, as final product of this production method

The centrifugal-multiroll system, as displayed schematically in figure 3.11, produces continuous fibers by passing the melted lava through several high-speed wheels in alternating direction of rotation. The fibers achieve a final diameter of 11 μm and 400 filaments[6] per toe.

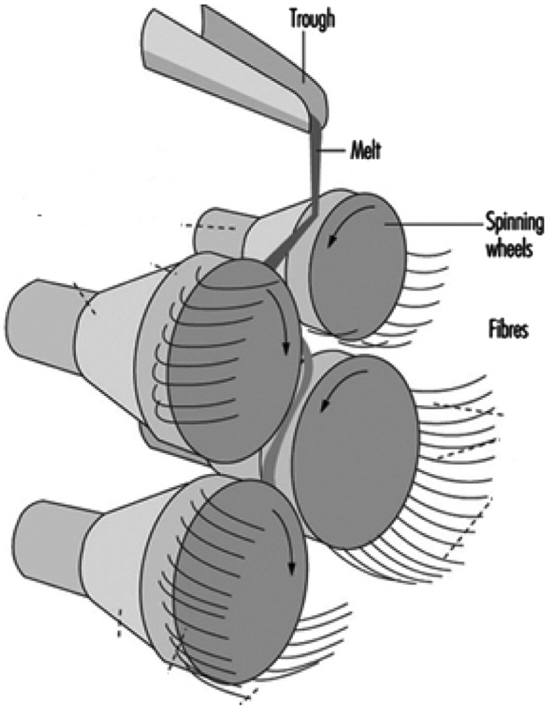

Figure 3.11 Centrifugal method for basalt production. Figure taken from[33]

As figure 3.11 shows, the centrifugal force exerted by the wheels to the melt forces the lava to pass through the array of the centrifugal wheels. These spinning wheels have to be placed such that they produce the desired diameter of the fibers.

3.2.4 Experiments conducted on basalt fibers

3.2.4.1 TGA tests

As table 3.4 shows, the fibers are composed by a series of oxides. Therefore, it is expected to observe a high temperature degradation of the basalt. This behavior was confirmed by the thermogravimetric analysis shown in figure 3.12. A sample of 18.32mg containing chopped fibers was placed in the apparatus (QA500, TA Instruments, USA). The sample was heated in a N_2-atmosphere at a rate of 25ºC/min from room temperature to 600ºC. As figure 3.12 shows, the curve can be regarded as a single-step mode. The value of the *onset* (i.e the temperature at which the sample starts to lose weight) is at 222ºC. This value is similar to the results found in other studies[27]. Additionally, the weight loss is very small (around 0.6%), which is also in agreement with the same study. It is important to note that the spectrum is characterized by a small fluctuating pattern (noise). This feature is characteristic of samples that possess a low mass to volume ratio, such as fibers. To improve the quality of the signal, the raw-data values obtained from the apparatus were filtered with a Gaussian window function.[8]. The two curves are superposed, showing a good fit between them.

Figure 3.13 shows the derivative of weight change (W%) with respect to temperature variation $\left(\frac{\Delta W\%}{\Delta T}\right)$ in units of $\left[\frac{\%}{{}^\circ C}\right]$ vs. temperature in $[{}^\circ C]$. This gives a more precise indication of the change in weight with the temperature. In this case, there are three clear peaks between 50ºC and 125ºC. These maxima correspond to water desorbed. The height of the peaks in the order of $10^{-3}\left[\frac{\%}{{}^\circ C}\right]$ integrated with the width of the peaks indicate a very small amount of water present in the fibers (around 0.05%). The highest weight loss of basalt fibers is around 40ºC higher than that of glass-fiber. This property of basalt is attributed to the spinning process and to the degree of cristallinity[13].

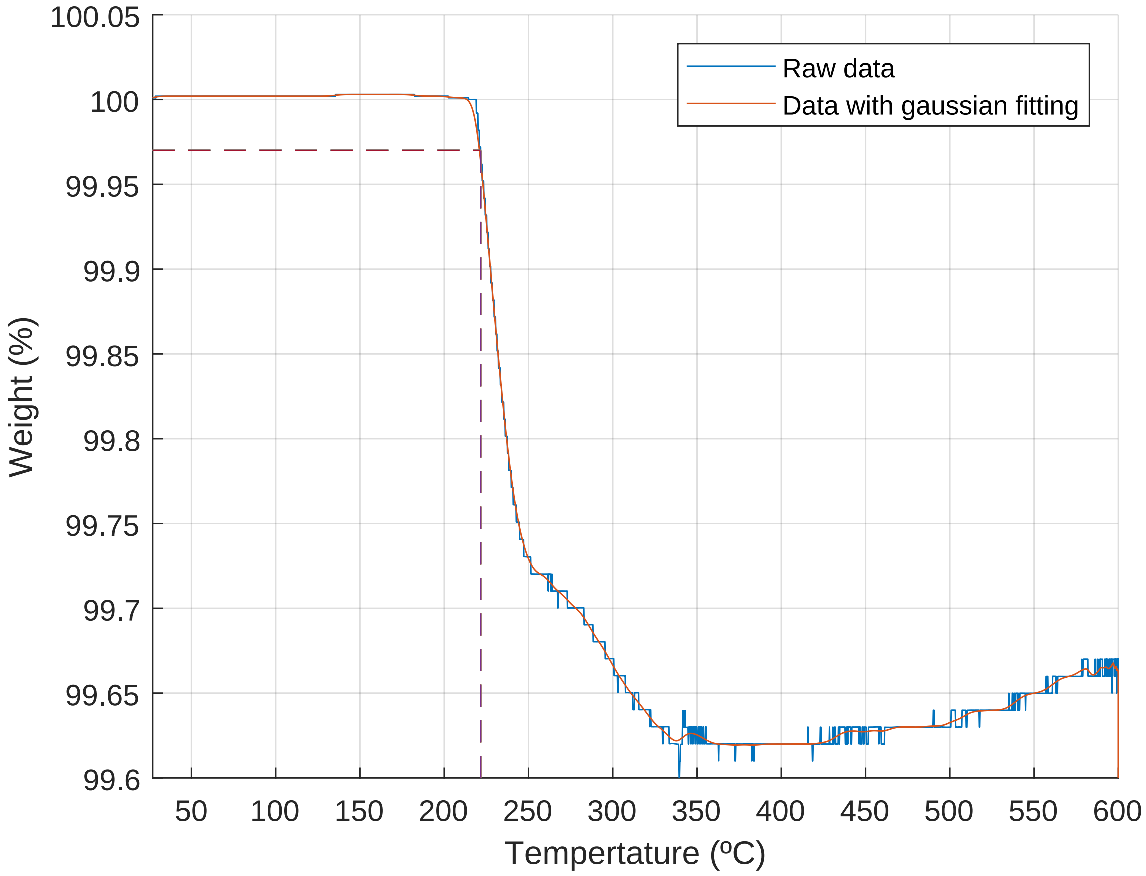

Figure 3.12 TGA of basalt fibers showing a single-step mode of weight loss.

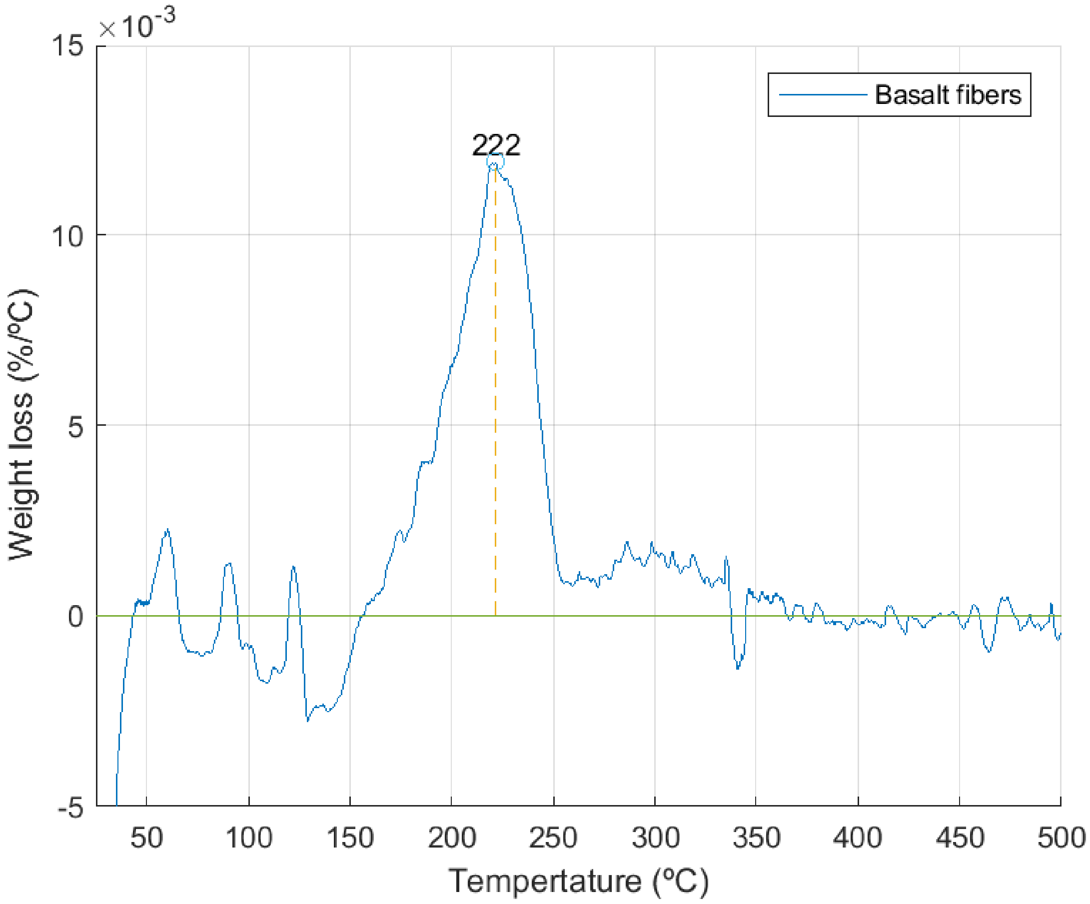

Figure 3.13 Differential TGA for the sample of figure 3.12. The main weight loss occurs at 222ºC.

3.2.4.2 Single fiber fragmentation test

Sample preparation In order to measure the adhesion of the basalt fibers with the epoxy matrix (previously described in equation 2.2), eight coupons were prepared with the dimensions shown in figure 3.14.

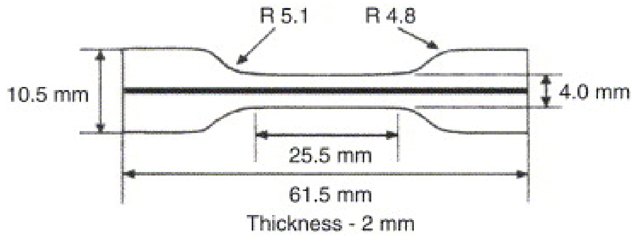

Figure 3.14 Coupon dimensions for SFFT[39]. Black line represents the fiber.

The mold used was made of flexible silicone, with an open end at the top. Before the mold was used, it was thoroughly cleaned with acetone and dried under the hood for ten minutes. Then, single basalt fibers were placed by hand on the mold cavities, such that the fibers would pass through the sprue slot. Each fiber was fixed to the mold by applying small drops of rubber cement (Elmer's Products, USA) with a syringe on the far ends of each sprue slot. After the rubber cement was applied, a stainless-steel spatula was used to roll the rubber cement and gently bring it to the sprue slot. It is important to note that after this step, the fiber should not be in tension. The mixed m-PDA and EPON-828™were degassed after being mixed (see chapter 2 for details) in a beaker together. The mold was also degassed to eliminate the air bubbles on the surface of the silicone-mold. The presence of bubbles in the cured coupon could create stress-concentrations in the samples, enabling cracks to propagate, and ultimately, causing the coupon to break at a lower stress. After the resin was degassed, a previously-heated glass-syringe was used to pour the resin into the mold. This tool is utilized because of the small volume of the mold cavities, as well as the fragility of one individual fiber. The mold with the resin was then placed in the oven for the curing step. It is important to maintain the surface of the mold horizontal so that the liquid resin flows evenly accross the cavity. When the samples are cured, they need to be polished by an automatic polisher to homogeneize the thickness of the sample (on the top and bottom sides). This processes ensures the surfaces are smooth so to avoid stress-concentrators. The eight samples were attached to the metallic disc with double-sided adhesive tape as shown in figure 3.15 and mounted into a metallurgical polisher machine (Struers Abramin Metal Polisher).

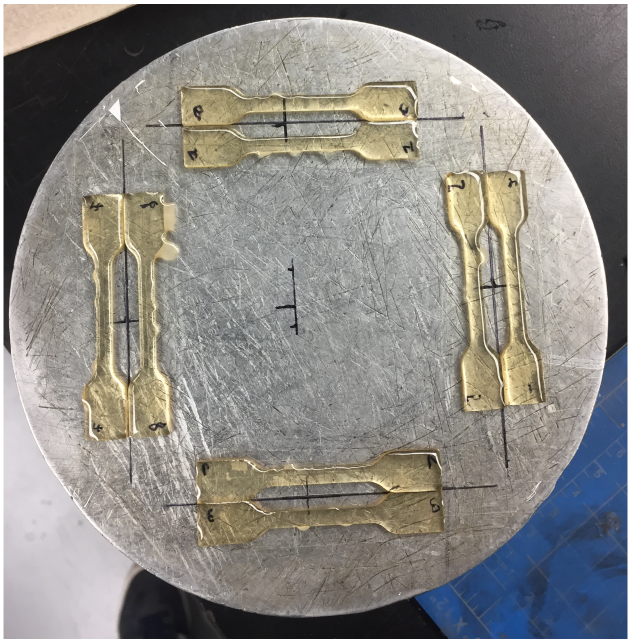

Figure 3.15 SFFT coupons mounted on metal surface for polishing.

The top surfaces of the samples have to face the polishing paper since the other side of the coupons (in contact with the mold) are very regular. Additionally, the samples that are in contact with one another should be oriented such that the end of greater thickness of one sample should be next to the end of smaller thickness of the sample. This set-up derives in a homogeneous polishing on all sides. Another important aspect to take into account is that the samples must be symmetrically oriented. This means that they have to be at the same distance from the midpoint of the disc to apply equal pressure on each sample. The coupons were polished using 320-, 600-, and 1200-ANSI-grit sizes for approximmately one minute with a force of 3-5N. The samples were then polished for 30 seconds with an alumina final polish abrasive.

Data collection One of the main parameters to assess the bonding strength of the fiber with the matrix is the fiber average diameter. To accurately determine this parameter, a calibrated micrometer slide was placed on each sample and observed with an optical microscope. The image of the scale on the slide of the microscope was projected to a real-time screen. Once this step was completed, the single fiber fragmentation test was conducted in the following way[54]:

The samples were placed under an optical microscope to measure the diameter of the embedded fiber in the epoxy. For this purpose, a micrometer calibration slide was placed on the coupon and the scalebar set on the screen of a real-time video apparatus. Then, the diameters were measured at different points of the coupon and the averaged diameter was calculated (see tables 3.5 and 3.6). The sample was fixed to the grips so that lateral displacements were prevented, but allowing the sample to have some space to move upwards and downwards. After this step a drop of oil was put on the middle of the sample. After the oil spread, a square glass slide of 18mm (see table 3.5) of side for the first four samples of side was placed on top of the sample. This thin slide was placed in the middle region of the coupon. For the second batch, a square glass slide of 22mm 3.5 was used. The reason to place the glass is to define a region to analyze. The use of oil is to prevent minimize the adhesion between the glass slide and the coupon, and thus, to measure the strain of the sample without other effects. The samples were subjected to tension by manually turning a screw on the tension stage in the axial direction, in increments of 0.0127mm. The extension was determined by the observing the dial. After applying the stress, the sample was visually scanned for fiber breaks and this number was recorded for each strain. By placing the sample between cross-polarizer, the double-reffracted light, called *birefringence* patterns are observed in the vicinity of every break. This effect called colloquially as *photoelasticity* originates from the distortion of light in materials subjected to strain. Furthermore, the shape of these patterns provide information about the adhesion between the fiber and the matrix and the failure mode of the fiber inside the coupon[12]. When the number of breaks remained constant after the sample was subjected to two increments of 0.0127mm, the sample was considered to have reached *saturation*. The break patterns were then recorded (using a camera connected to an optical microscope under polarized light). These break patterns are displayed in figures 3.17 at low magnification and 3.17 at high magnification. The fiber breaks -see dark regions in figure 3.16- are surrounded by birefringence (bright regions sorrounding the breaks). The horizontal length of the break is known as the break gap. This length varies depending on the applied stress. Another crucial information that the shape of the birefringence is the bonding with the matrix. A flat, elongated birefringence indicates that the stress has been poorly transfered from the fiber to the matrix. This can be explained by the behavior of the interface between the fibers and the matrix. After curing of the sample, the matrix is bonded with the fiber at a molecular level[36]. When the sample is subjected to tensile stress, the fiber should transfer this load to the epoxy. If the bonding of the fiber with the resin is high, the interface region in the vicinity should show signs of stress. In the case of a basalt fiber in epoxy, the birefringences indicate that the fiber has experienced *debonding* while breaking, i.e., there is a poor adhesion of the fibers with the matrix. The *debonding zone* is referred as the bright regions around a fiber break. Note that the fiber breaks appear as dark under polarized light because there is no stress at those spots.

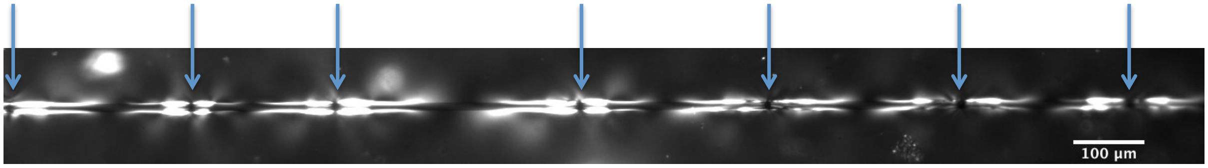

Figure 3.16 Micrograph of basalt fiber under polarized light in epoxy showing several breaks. Image taken at saturation strain. Arrows indicate fiber breaks.

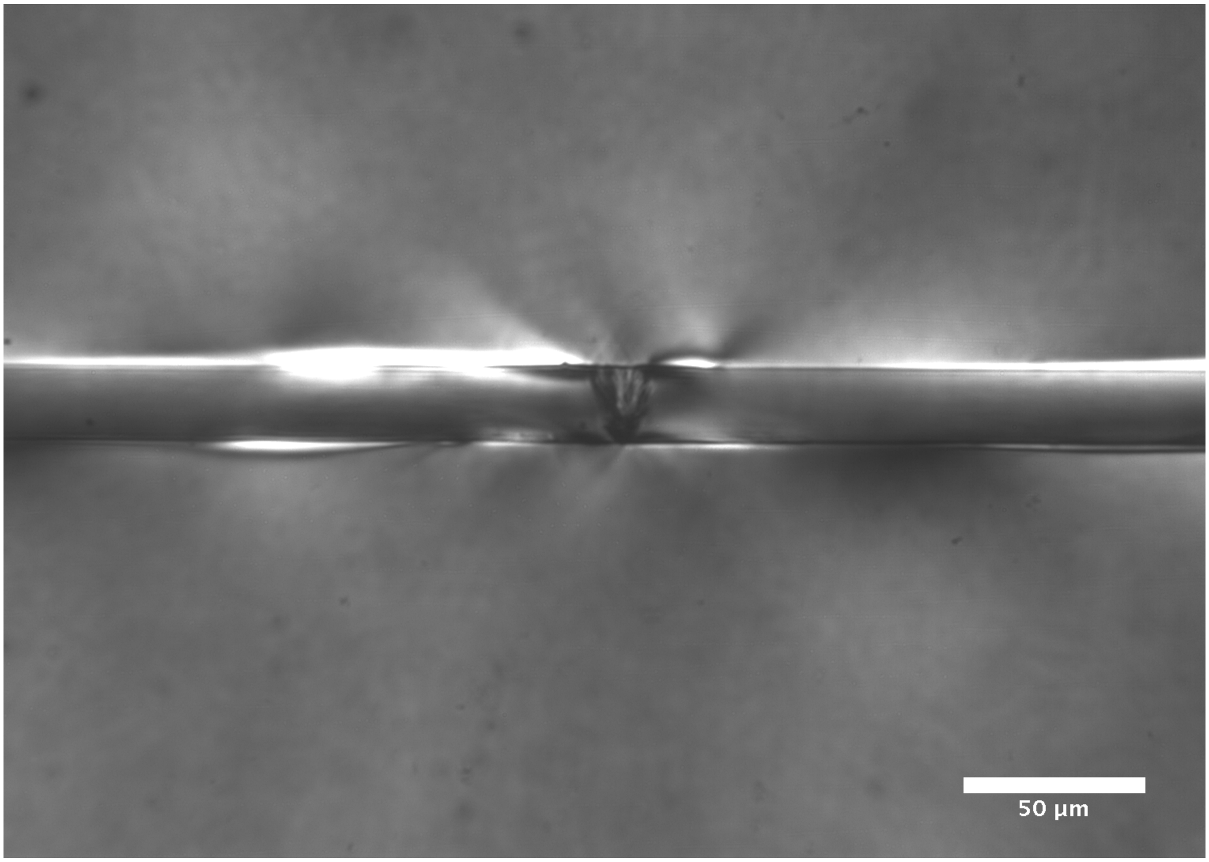

Figure 3.17 Region of basalt fiber break in epoxy at saturation strain under polarized light. The fiber has experienced debonding at break.

The following tables (3.5 and 3.6) display the summarized results of the SFFT conducted in this study:

Table 3.5 Single fiber fragmentation test of basalt fibers in epoxy (number of breaks measured in a span of 18 mm)

Strain $\left(\frac{\mathrm{mm}}{\mathrm{mm}}\right)$	**Number of breaks**			
	Sample 1	Sample 2	Sample 3	Sample 4
	$\bar{d} = 11.67\ \mu\mathrm{m}$[a]	$\bar{d} = 12.07\ \mu\mathrm{m}$	$\bar{d} = 12.93\ \mu\mathrm{m}$	$\bar{d} = 14.47\ \mu\mathrm{m}$
0.00282	0	0	0	0
0.00353	0	0	0	0
0.00423	0	0	0	0
0.00494	0	0	0	0
0.00564	0	0	0	0
0.00635	0	0	0	0
0.00706	0	0	0	0
0.00776	0	0	0	0
0.00847	4	4	1	1
0.00917	9	7	5	5
0.00988	26	10	7	12
0.01058	30	16	9	22
0.01129	44	22	11	27
0.01199	48	break	18	30
0.01270	52	-	28	break
0.01341	52	-	34	-
0.01411	54	-	35	-
0.01482	54	-	break	-
0.01552	break	-	-	-

[a]: $\bar{d}$ is the average diameter of the fiber measured at different points of the coupon

Table 3.6 Single fiber fragmentation test of basalt fibers in epoxy (number of breaks measured in a span of 22 mm)

Strain $\left(\frac{\mathrm{mm}}{\mathrm{mm}}\right)$	**Number of breaks**			
	Sample 5	Sample 6	Sample 7	Sample 8
	$\bar{d} = 8.900\ \mu\mathrm{m}$[a]	$\bar{d} = 11.03\ \mu\mathrm{m}$	$\bar{d} = 11.03\ \mu\mathrm{m}$	$\bar{d} = 10.80\ \mu\mathrm{m}$
0.00231	0	0	0	0
0.00288	0	0	0	0
0.00346	0	0	0	1
0.00404	0	0	0	2
0.00462	2	8	0	2
0.00520	2	18	0	3
0.00577	8	27	0	7
0.00635	10	39	0	10
0.00693	21	49	0	14
0.00750	27	51	0	25
0.00808	39	55	0	34
0.00866	57	57	2	43
0.00924	62	60	3	48
0.00981	break	60	7	break
0.01039	-	-	13	-
0.01100	-	-	30	-
0.01154	-	-	43	-
0.01212	-	-	48	-
0.01270	-	-	51	-
0.01328	-	-	57	-
0.01385	-	-	break	-

[a]: $\bar{d}$ is the average diameter of the fiber measured at different points of the coupon

The data from the tables 3.5 and 3.6 are summarized in the following image (figure 3.18).

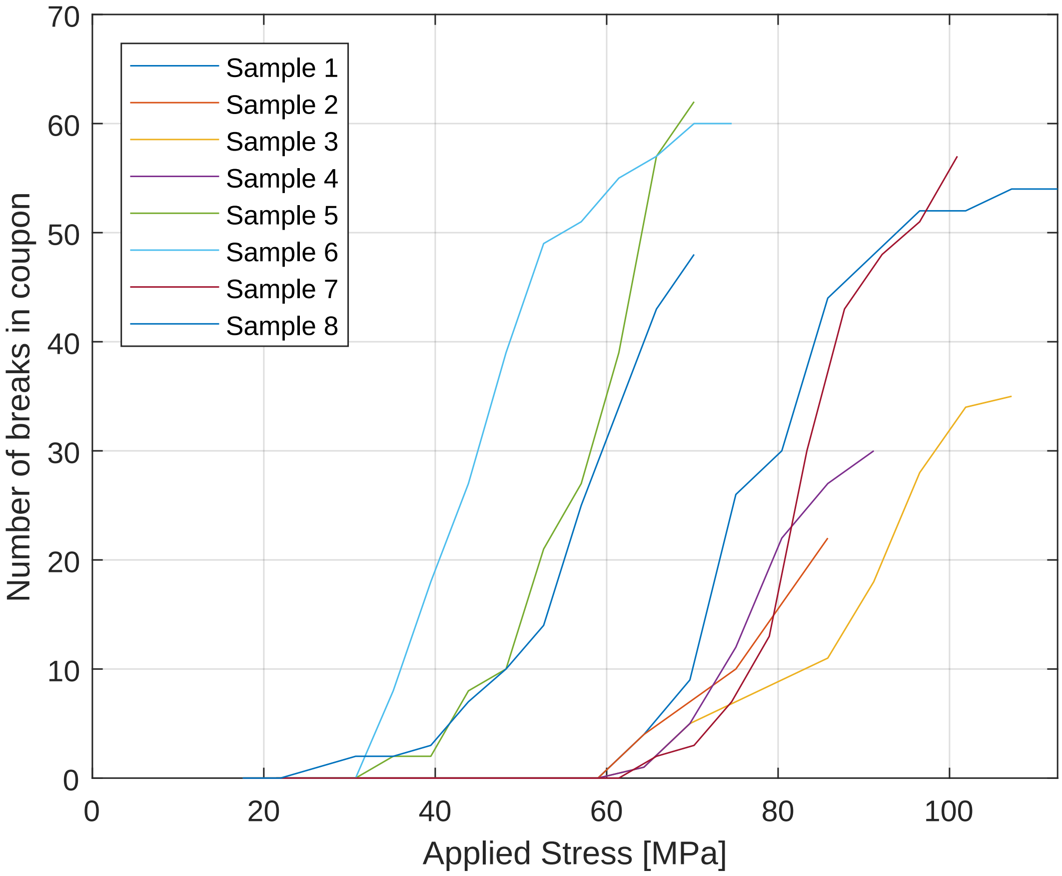

Figure 3.18 Breaks with respect to strain

The shape of the behavior of the number of breaks with respect to the applied strain resemble a Weibull distribution as reported in previous works[20] [55]. Furthermore, the distance of between each break is not constant, as figure 3.16 shows. Therefore, the results are analyzed using the following guidelines.

Data analysis The interfacial shear strength between the fiber and the epoxy matrix is given by the equation proposed by Kelly and co-workers[35]:

$$\tau = \frac{\sigma_F d}{2l_c} \tag{3.5}$$

where τ is the interfacial shear strength, σ the fiber tensile strength, and l_c the critical length of the fiber. l_c is determined as

$$l_c = \frac{4}{3}\bar{l} \tag{3.6}$$

where $\bar{l}$ is calculated as the gauge length divided by the number of breaks at the critical strain. With this approach the IFFS gives a mean value of 9.60MPa with a SE of ±0.77MPa. Since the critical length is subjected to considerable variation due to flaws of the fiber, handling of the specimen, etc.[51], the critical length determination is established with a probablilistic approach[23]. Ultimately, this method is used estimation of the interfacial shear strength. The following equation (as proposed by Drzal et al.[20]) predicts the IFFS of basalt in the epoxy matrix:

$$\tau = \frac{\varepsilon E_f}{2\beta}\Gamma\left(1 - \frac{1}{\alpha}\right) \tag{3.7}$$

where ε is the measured strain in $\frac{\text{mm}}{\text{mm}}$, E_f the nominal modulus of basalt (in MPa), β the shape parameter and α the scale parameter of the Weibull distribution and Γ the gamma function[55]. This probabilistic approach yields a mean value for the interfacial shear strength of 9.73MPa with a standard error of ±0.75. For the failure probability, a two-parameter Weibull probability density function $f(\varepsilon, \alpha, \beta)$ of the random variable ε of the form:

$$f(\varepsilon;\alpha,\beta) = \frac{\alpha}{\beta}\left(\frac{E_f\varepsilon}{\beta}\right)^{\alpha-1} exp\left[-\left(\frac{E_f\varepsilon}{\beta}\right)^{\alpha}\right] \tag{3.8}$$

is used. The cumulative probability function $F(\varepsilon;\alpha,\beta)$ for this distribution is obtained by integrating equation 3.8. This means:

$$F(\varepsilon;\alpha,\beta) = \int_{-\infty}^{X} f(\varepsilon;\alpha,\beta)d\varepsilon \tag{3.9}$$

Last equation yields:

$$F(\varepsilon;\alpha,\beta) = 1 - e^{\left(-\frac{\varepsilon}{\alpha}\right)^{\beta}} \tag{3.10}$$

In order to assess the correctness of this distribution, the data obtained from the SFFT were plotted in figures 3.19 and 3.20. These two plots were generated in MATLAB™and the plots are shown in two separate figures for clarity. As it can be seen, the dots (which represent the actual data) are in very good agreement with the predicted line (shown as discontinuous lines).

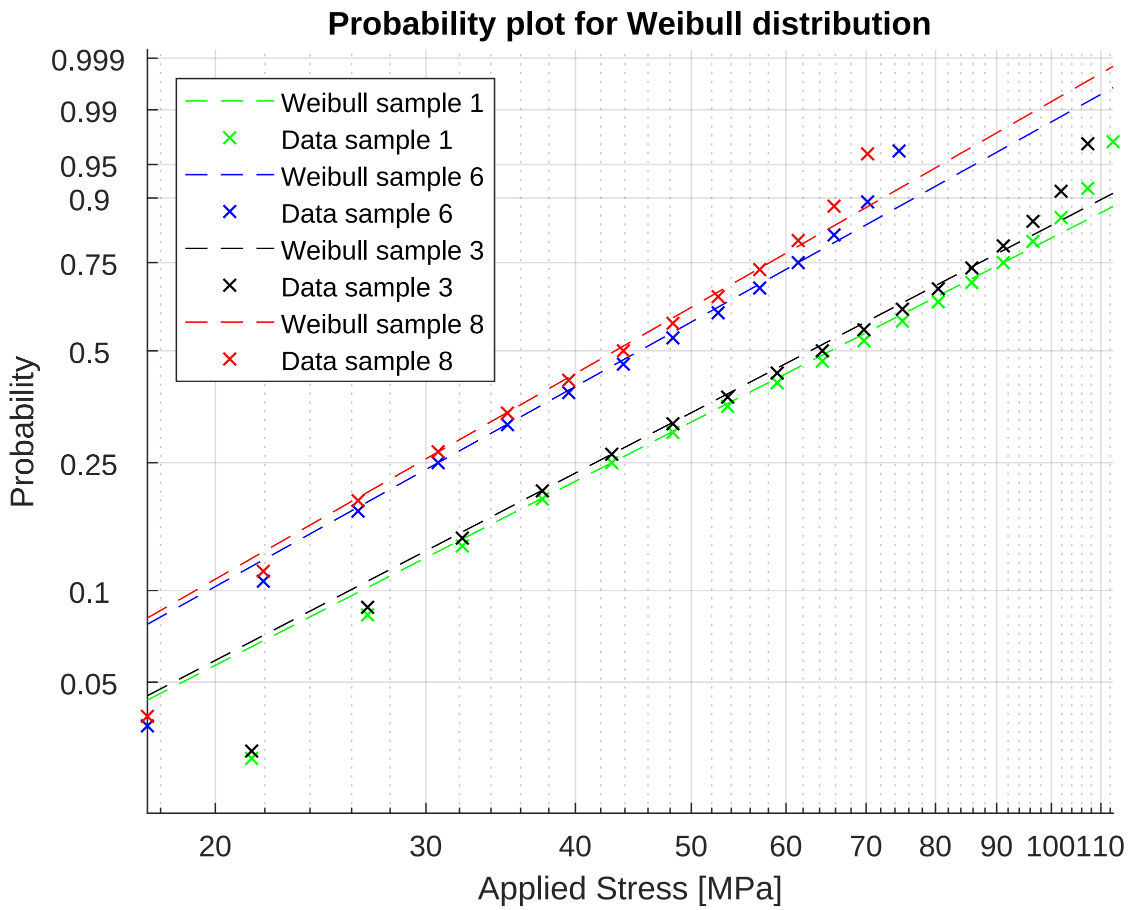

Figure 3.19 Weibull fit for SFFT test of four samples

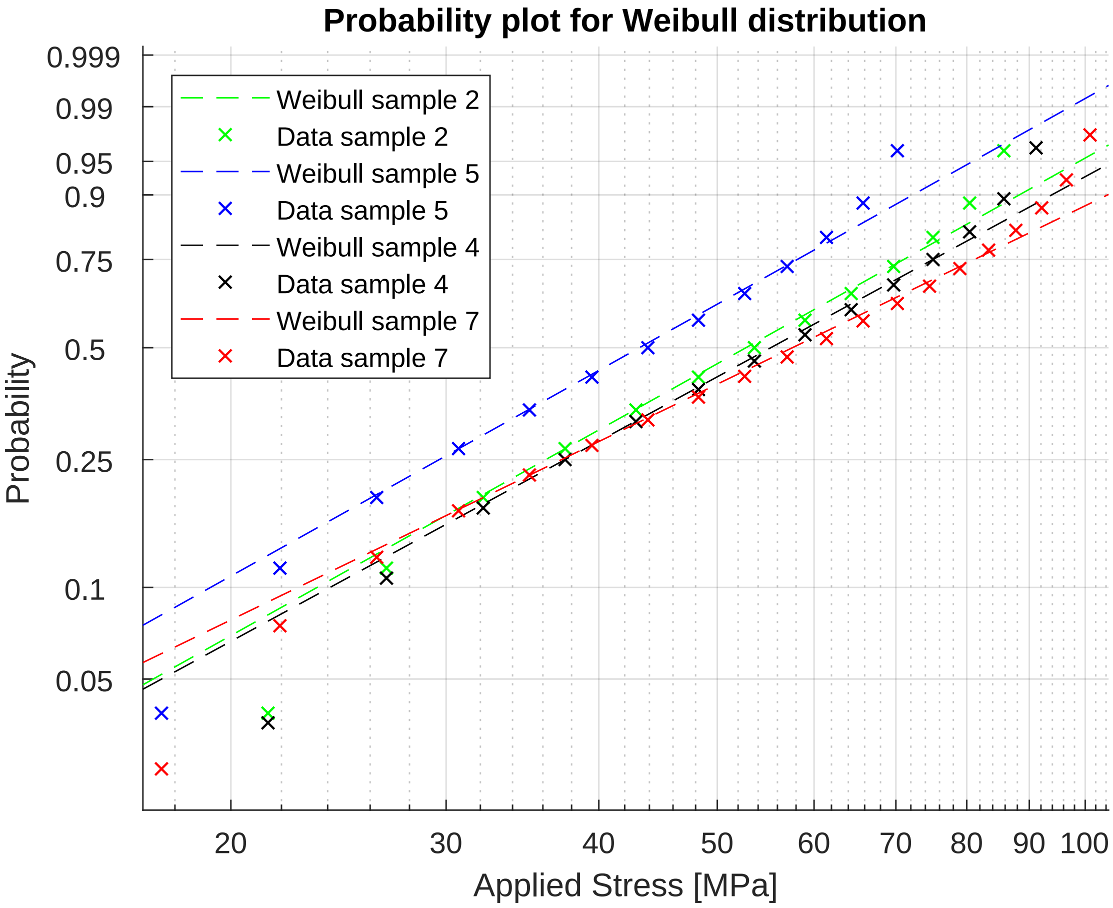

Figure 3.20 Weibull fit for SFFT test of the other four samples

CHAPTER 4

COMPOSITE CHARACTERIZATION

4.1 Neat epoxy characteristics

The resin selected for all of the composites used in this study was Ddiglycidyl ether of bisphenol A (DGEBA - EPON 828 - Miller Stephenson Company,USA) with meta-phenylene diamine (mPDA) as curing agent (Sigma Aldrich, USA). The ratio was 100/14.5 DGEBA/mPDA by weight. This matrix in this stoichiometry was selected due to the fact that this epoxy has been very well characterized for its mechanical and physical properties. The density of the matrix is 1.90 $\frac{g}{cm^3}$[38], a flexural strength of 120MPa and elastic modulus of 3.2GPa[19]. The curing cycle of the mixture was done 75ºC for one hour and a post-curing at 125ºC for two hours. The curing and post-curing processes were conducted in a convection oven. Neither the resin nor the curing agent were treated in any way. They were used as received.

4.2 Procedure for the fabrication of composites

The following method was implemented for the fabrication of all unidirectional flexural composites analyzed in this study. The mould consisted of two stainless-steel plates of dimensions 150mm x 150m x 5mm. Two square pieces of aluminum foil were cut in dimension of 16cm x 16cm. The aluminum foil was used to cover the plates, leaving 1 cm from each of the stainless-steel plate so that the aluminum foil could be folded to leave a flat surface to be in contact with the resin. After this step, both plates (covered with aluminum foil) were put between flat steel plates of 20kg each to improve flatness of the surfaces of the mold. After two hours under pressure, an U-shaped high-temperature silicone rubber sheet is attached with high-temperature adhesive tape to one side of the mold (see red U-shaped region in fig.4.1). Additionally, two silicone rubber strips are adhered to the mold in order to set the with of the composites. When this step is completed, mold release liquid is applied on the aluminum-covered stainless steel plate and to the silicone rubber. The mold release has to be applied with a paper towel. The application of this liquid is first applied vertically. After one minute, the mold release is dried with a paper-towel horizontally. The mold release prevents the cured resin to adhere to the mold and to the rubber. It has to be done under a specially designated hood in order to prevent contamination. After five minutes the fibers (see brown region in fig.4.1) were manually aligned and held in place with two strips of high-temperature adhesive on top and bottom (see blue features in fig.4.1). The other stainless-steel plate was aligned and tightened with C-clamps on the four sides of the plates. The C-clamps serve to compress the silicone rubber to achieve a gap of 3.2mm which is the desired thickness (depth) for the dimension of the ASTM 790 standard. By doing this a mold with an open end on top is achieved. The mold is placed in a convection oven at 75ºC for hour oriented as figure 4.1 shows.

Along with the mold, one plastic beaker with 100g resin (DGEBA) and another with 14.5g of the curing agent (m-PDA) were placed in a convection oven for one hour at 75ºC. Then, the resin is poured in the beaker containing the m-PDA and stirred for one minute, assuring that the resin on the walls of the container are transferred to the other beaker. After this, the mixture of DGEBA with m-PDA is brought back to the beaker that originally contained the resin. The liquid mixture is stirred again for one approximately one minute. At this point, around 30g of the mixture is poured into the mould, in both gaps between the silicone rubber and also over the fibers. The mold should be oriented while pouring the mixture as shown in fig.4.1. The space between the silicone rubber strips and the bottom of the U-shaped rubber enables the liquid resin to wet the fibers. Then, the mold the the beaker containing the rest of the mixture are brought to a vacuum oven at 75ºC, with the mold oriented as shown in the figure. When vacuum is applied the liquid mixture wets the fibers and degasses the mixture. Vacuum should be applied for around three to five minutes, until the bubbles that initially formed on the surface have grown and collapsed. This step is necessary to remove air bubbles while promoting substantial mixing of the resin with the curing agent[24]. The mold and the beaker were brought back to atmospheric pressure when the small bubbles started to form at the bottom of the beaker and rise. This is an indication of the process of evaporation of the constituents that may interphere with the curing process of the epoxy and, ultimately, with the physical and mechanical properties of the composite. When the degassing was completed, the liquid mixture was poured over the fibers several times, in order to allow the fibers to be fully wetted. Additionally, the mixture was poured in both segments of the mold without fibers to promote the flow of the resin to the fibers.

At this point, the mold with the resin was placed in a convection oven (previously set to 75ºC) and kept at 75ºC for two hours. After this time has passed the temperature is increased to 125ºC and kept for two hours for the post-curing process. When this cycle is complete the oven with the sample inside should be turned off so that the internal temperature of the oven reaches room temperature. This step takes approximately four hours.

The composites were then cut to specimens of dimensions to meet the standards for flexural testing of reinforced plastics (ASTM-D790[63]). It was not necessary to polish the samples after before testing them since the surfaces of the specimens were smooth and regular in cross-section.

4.3 Evaluation of composites

4.3.1 Three-point bending tests

The three-point bending tests were conducted in compliance with ASTM-D790[63] with a United Testing Systems (UTS) apparatus model SFM-20. The following parameters were calculated for each batch of samples in compliance with[63]:

- The span (L) was calculated as 16 times the width of the specimen
- The termination of the test when the midspan deflection has reached $0.05\left(\frac{\text{mm}}{\text{mm}}\right)$. This value is calculated with the following equation:

$$D = \frac{rL^2}{6d} \tag{4.1}$$

where r = 0.05 (strain in $\frac{\text{mm}}{\text{mm}}$), and d the thickness of the sample (referred as depth in ASTM-D790).

- The rate of the cross-section motion R in $\left(\frac{\text{mm}}{\text{min}}\right)$, calculated with

$$R = \frac{ZL^2}{6d} \tag{4.2}$$

where Z = 0.01 is the rate of straining of the outer fiber in $\left(\frac{\text{mm}}{\text{mm min}}\right)$

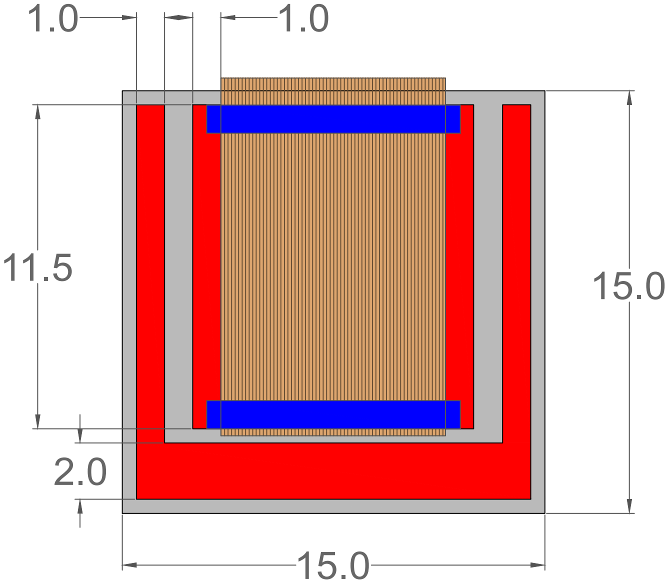

Figure 4.1 Mold scheme used to prepare flexural coupons.

Figure 4.2 Bamboo (AFEX) cut to a length of 12.7 cm.

Figure 4.3 Basalt fibers cut to a length of 12.7 cm.

Figure 4.4 Basalt and bamboo fibers intertwined and cut to a length of 12.7 cm.

4.3.2 Fiber distribution and void content assessment

The following procedure was conducted to visually evaluate features of the composites such as the distribution of the fiber-bundles, the presence of voids and the amount of the different components of the bamboo fibers (see chapter 3). The flexural composites were cut through the thickness (perpendicular to longest dimension of the sample) to obtain four samples of same dimensions. This was done in order to have representative cross-section observations of the composite. After the samples were cut, they were placed in a cylindrical holder for polishing, such that the cross-sections would be exposed to the polishing surface. A long-cure epoxy in a weight ratio of 100g resin to 14g of hardener (LC Epoxy, LECO Corporation, USA) was used to hold the pieces of the sample in place. The sample was allowed to cure at room temperature overnight. After this, the cured epoxy containing the sections of the composite were placed in a vibratory polisher (VibroMet I™,Buehler, USA) for three hours.

4.4 Bamboo composites

4.4.1 Introduction

The next step of the present study was the fabrication (see section4.2 for details on the procedure) of composites with AFEX-treated bamboo fillers in an epoxy-based matrix. There were three batches produced with different bamboo weight percet composites with different fiber content were fabricated. Additionally, a first attempt to use bio-based (Acrodur™-950L, BASF, Germany) resins for the fabrication of bamboo-reinforced composites is reported in Appendix 5.2.3. These composites were not further evaluated in the present study. All the following experiments were conducted with epoxy resin (DGEBA + mPDA) as matrix.

The fabricated composites exhibited a good dispersion of the fibers as displayed in 4.5. This sample was prepared in accordance to the method described in section 4.3.2. The image was acquired via a transmission optical microscope (Keyence, USA) in a grey-scale mode to improve the contrast between the fibers with the epoxy.

In order to understand the hybrid synergistic effect of the combination of basalt and bamboo fibers, unidirectional bamboo samples were first prepared. This procedure was conducted in order to understand first the interactions of the bamboo fibers with the matrix and then infere their performance when combined with basalt. The current section studied the mechanical response to three-point bending tests. It is expected that the increase of the bending strength of the composite is, primarily, due to the interfacial shear strength of the fibers in the composite[66].

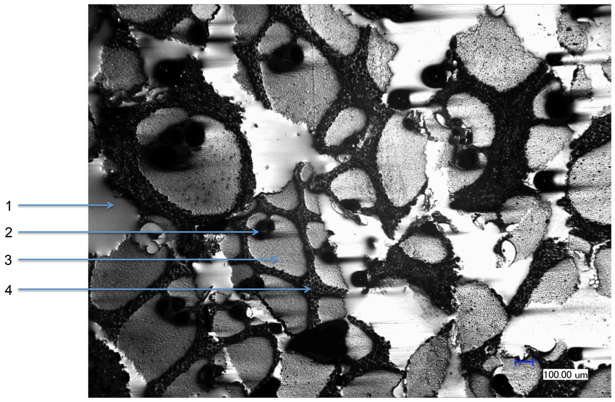

Figure 4.5 Transmitted light micrograph of cross-section of bamboo composite (40 weight % of fibers).1: resin, 2:hollow-vessel region, 3: fiber-sheath of sclerenchyma cells, 4: parenchyma cells. Note good dispersion of fibers.

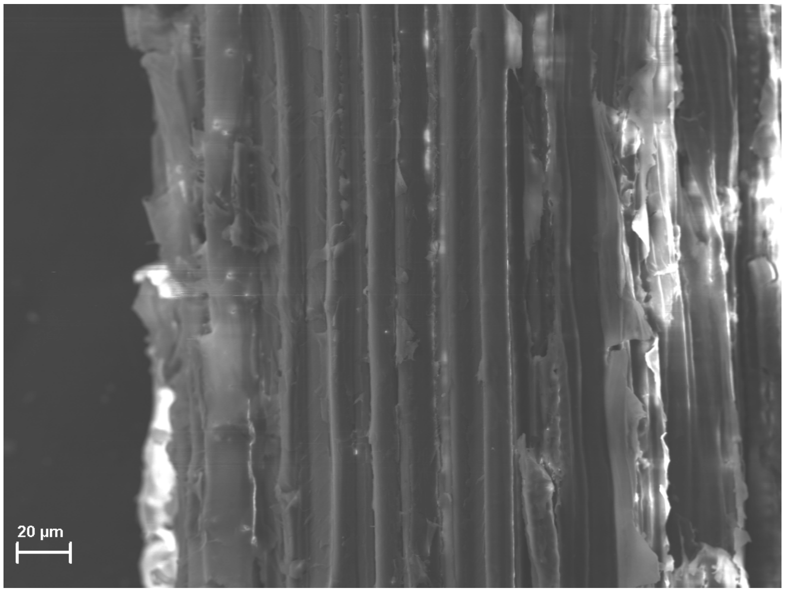

Figure 4.6 Surface of fiber bundles in composite (40 weight %) showing resin residues on the fibers.

4.4.2 Physical and mechanical properties

Mechanical properties[22]

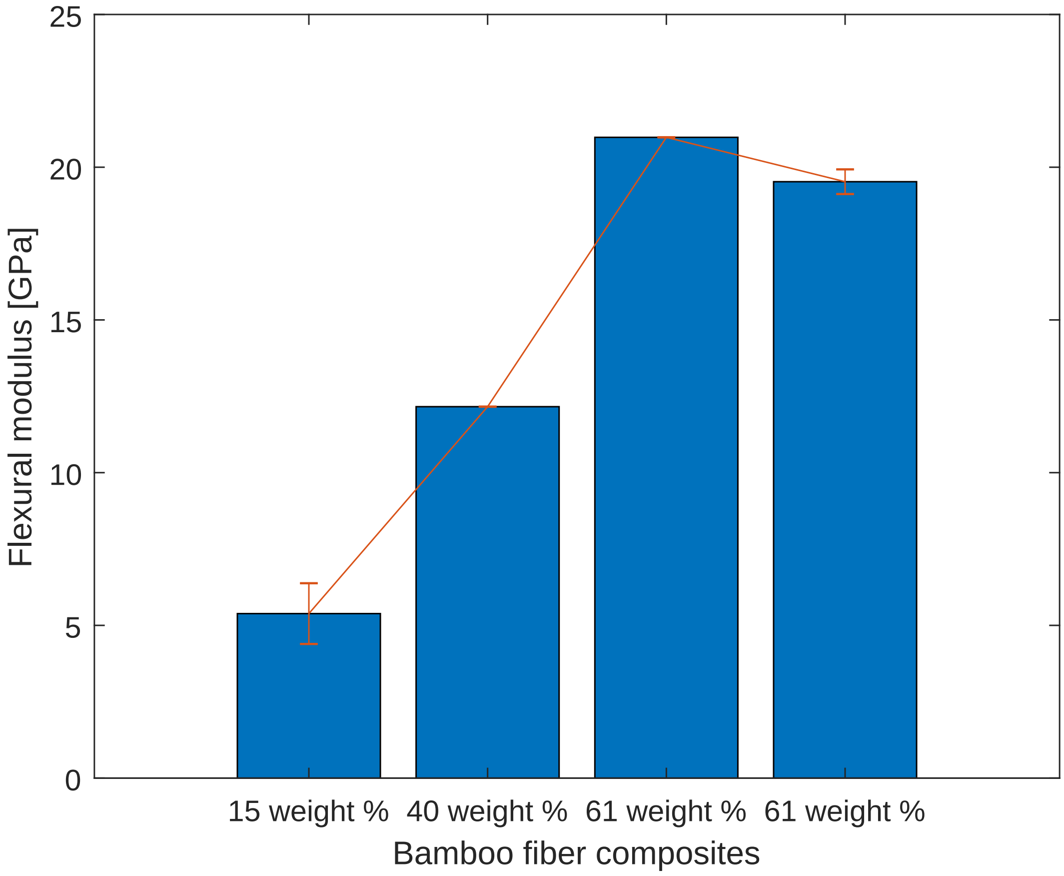

Figure 4.7 Elastic modulus of bamboo-reinforced composites with different weight fraction of fibers.

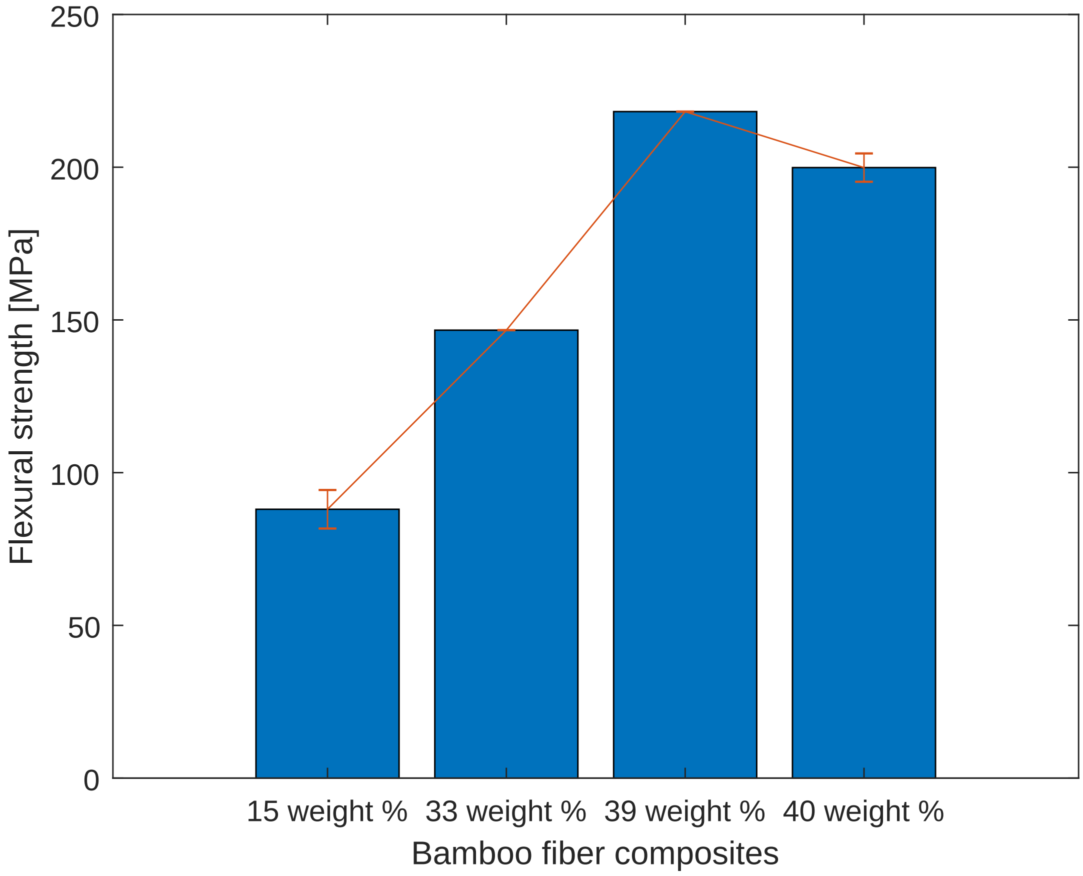

Figure 4.8 Flexural strength of bamboo-reinforced composites at several values of fiber content.

4.4.3 Fracture analysis

The bamboo fiber in fig.4.9 shows clear evidence of epoxy on the surface, a characteristic that shows good interfacial bond strength. Furthermore, the matrix in fig.4.11 presents features of *river patterns* which are evidence of high interfacial bonding. These features are also clear in the resin-rich region of fig.4.12. The layered structure formed in this figure in the vicinity to the fiber-bundles indicate fiber pull-out under tension[29].

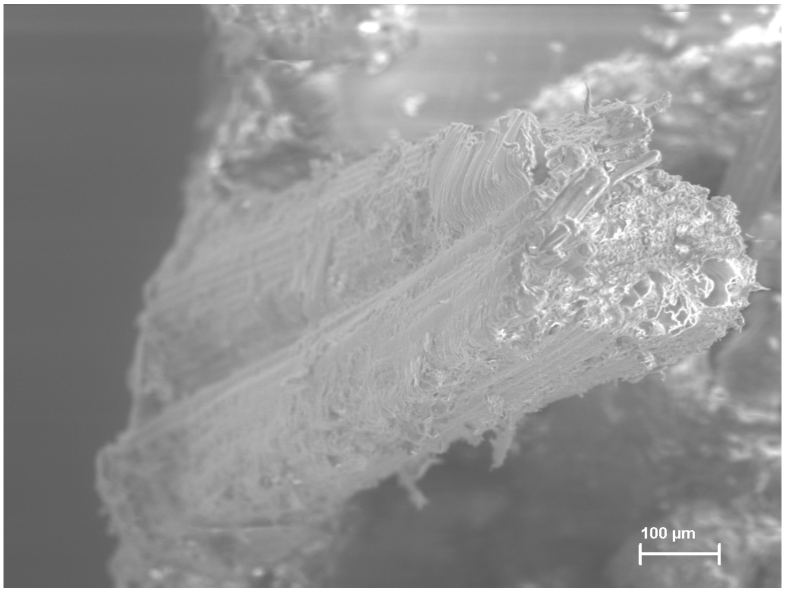

Figure 4.9 Bamboo fiber bundle in tension side of composite (40 weight %) Note epoxy on the surface of bamboo.

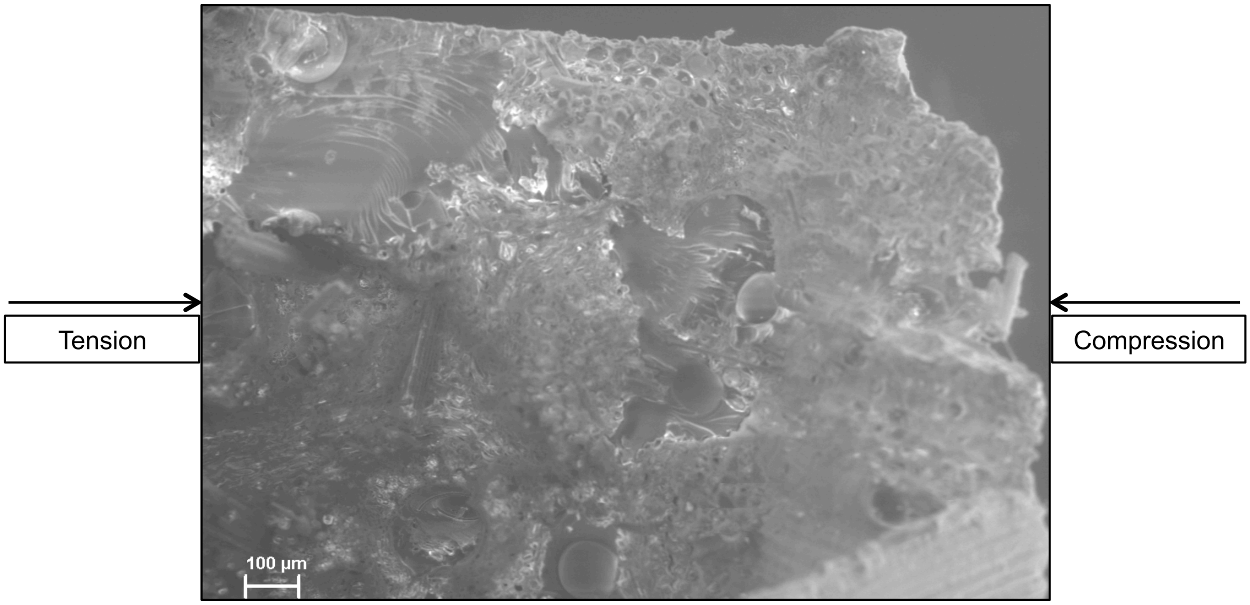

Figure 4.10 Fracture surface of bamboo-reinforced composite. Resin deformation observable on top left side. Fibers broken, not pulled out of the matrix.

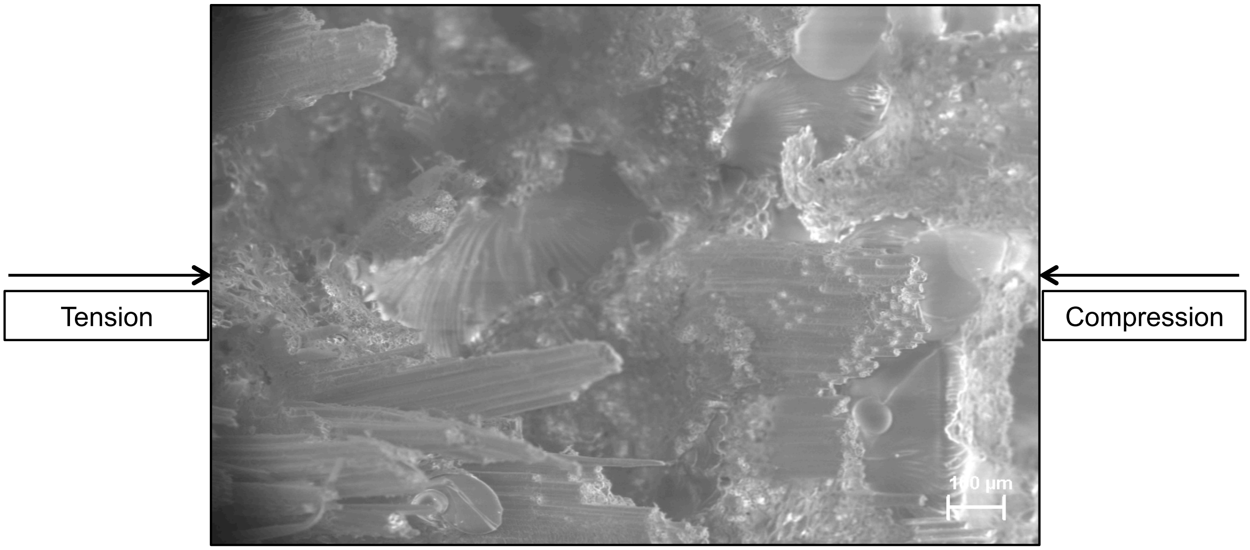

Figure 4.11 Fracture surface in center of sample. Different heights of fibers' breaks indicate energy absorption.

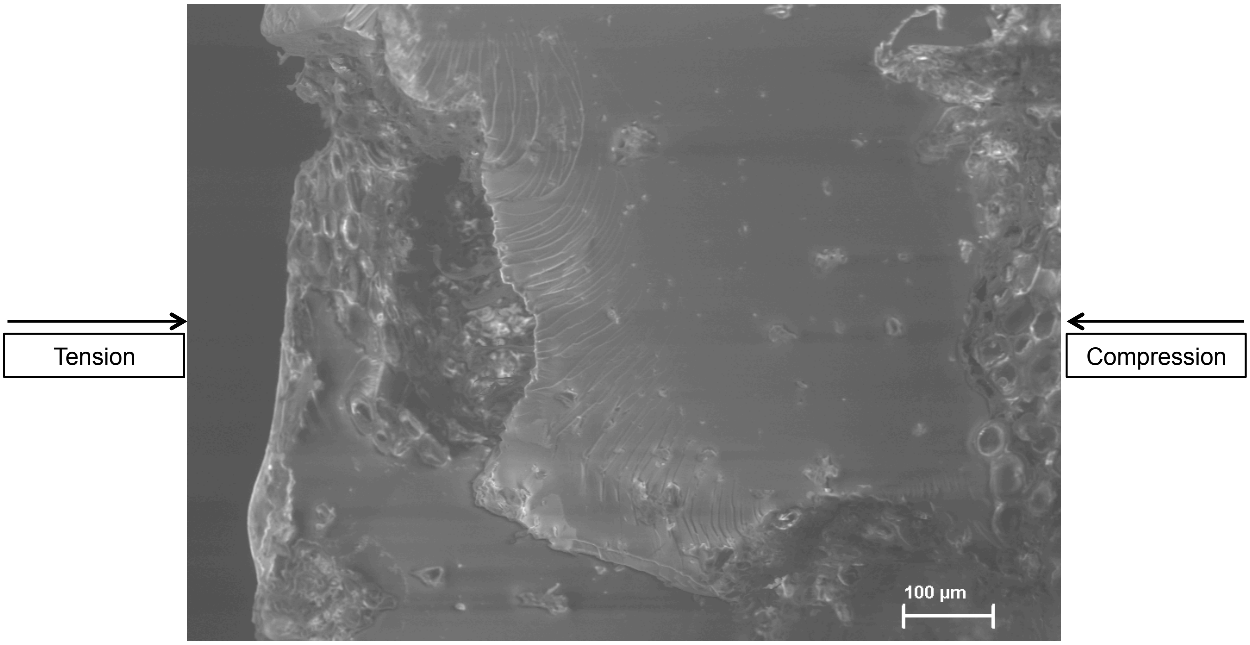

Figure 4.12 Fracture surface of bamboo-reinforced composite on tension side (40 weight %). Hackle formation and river patters on resin surface. Debris indicate tensile failure of fiber.

4.5 Basalt composites

4.5.1 Introduction

In order to investigate the behavior of basalt fibers as reinforcement agents in an epoxy-based matrix, composites with different fiber content were fabricated. All the samples were produced using the technique described in section 4.2. This technique was proved to be adequate for a good dispersion of this type of fibers as is observed in figure 4.13. The concentration of fibers in certain areas can be explained by means of the fact that they were not treated in any way before the composite fabrication, so a possible explanation is the poor adhesion between the fibers and the matrix. This micrograph shows a region of the cross-section of a basalt-reinforced composite (50 weight percent of fibers). This sample was prepared in accordance to the method described in section 4.3.2. The image was acquired via a transmission optical microscope (Keyence, USA) in a mode of scales of grey to enhance the contrast between the fibers (dark circular spots) and the light-grey matrix. The two dark irregular spots that are visible in the image are due to the reflection of the light through the specimen and do not represent a feature of the composite.

Since the ultimate goal of the present study is to understand the properties of the hybridized composites (bamboo/basalt reinforced composites), it is imperative to understand the characteristics of basalt composites. This section is dedicated to the understanding of the mechanical properties of basalt-reinforced composites subjected to three-point bending tests with the hope to elucidate the synergetic effect of the combination of bamboo and basalt as fillers.

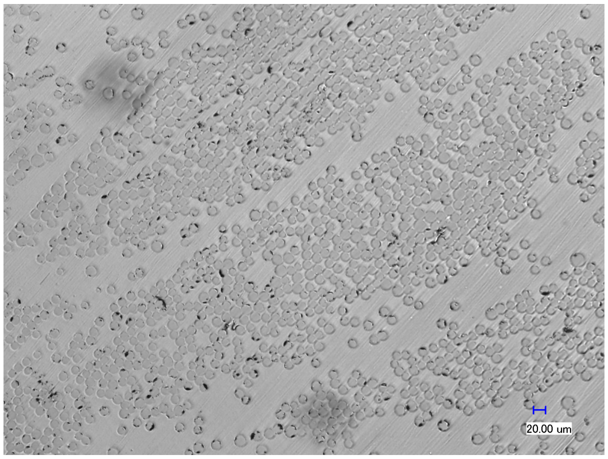

Figure 4.13 Cross section of basalt composite (50 weight %). Note good dispersion of fibers.

4.5.2 Results on flexural tests

The three-point bending tests were conducted in compliance with the ASTM D-790 standard as described in detail in section 4.3. A series of four samples for each batch of the same composition was produced. The flexural strength and modulus were calculated. A summary of these properties is presented in the figures 4.14 and 4.15.

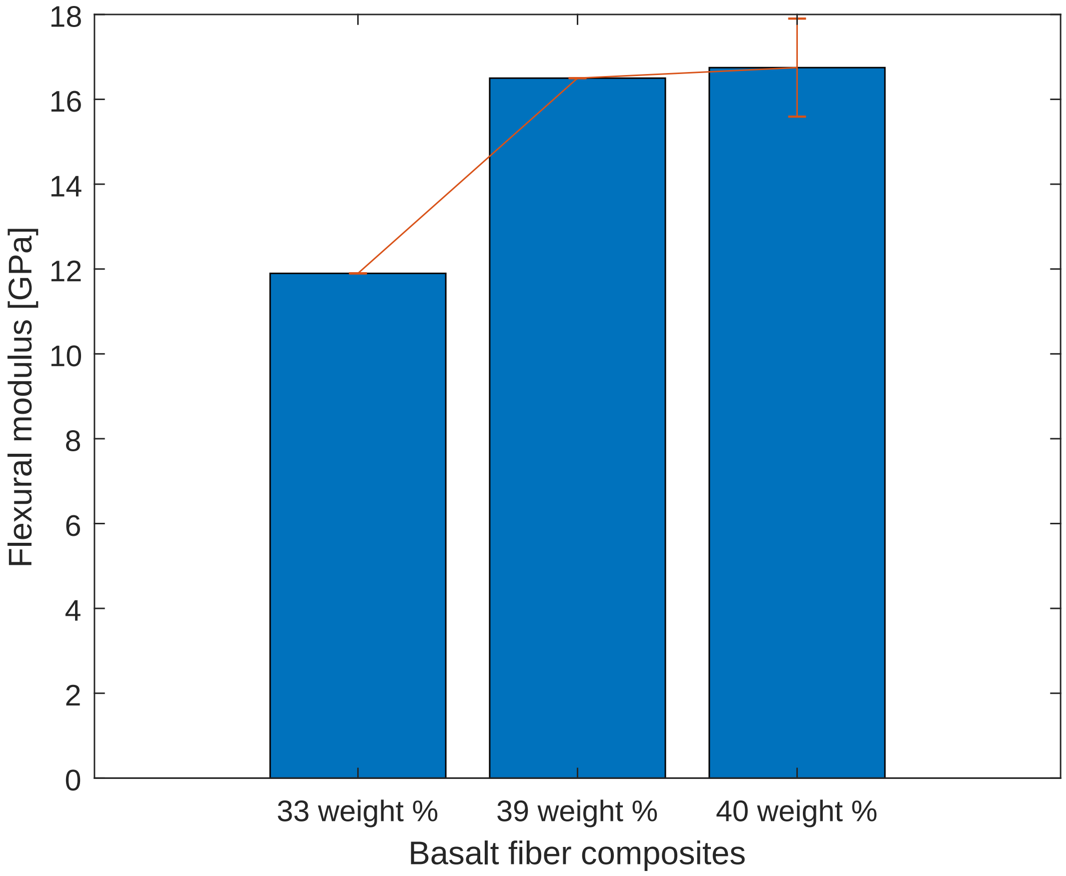

Figure 4.14 Elastic modulus of basalt-reinforced composites with different weight fraction of fibers. Basalt fibers untreated.

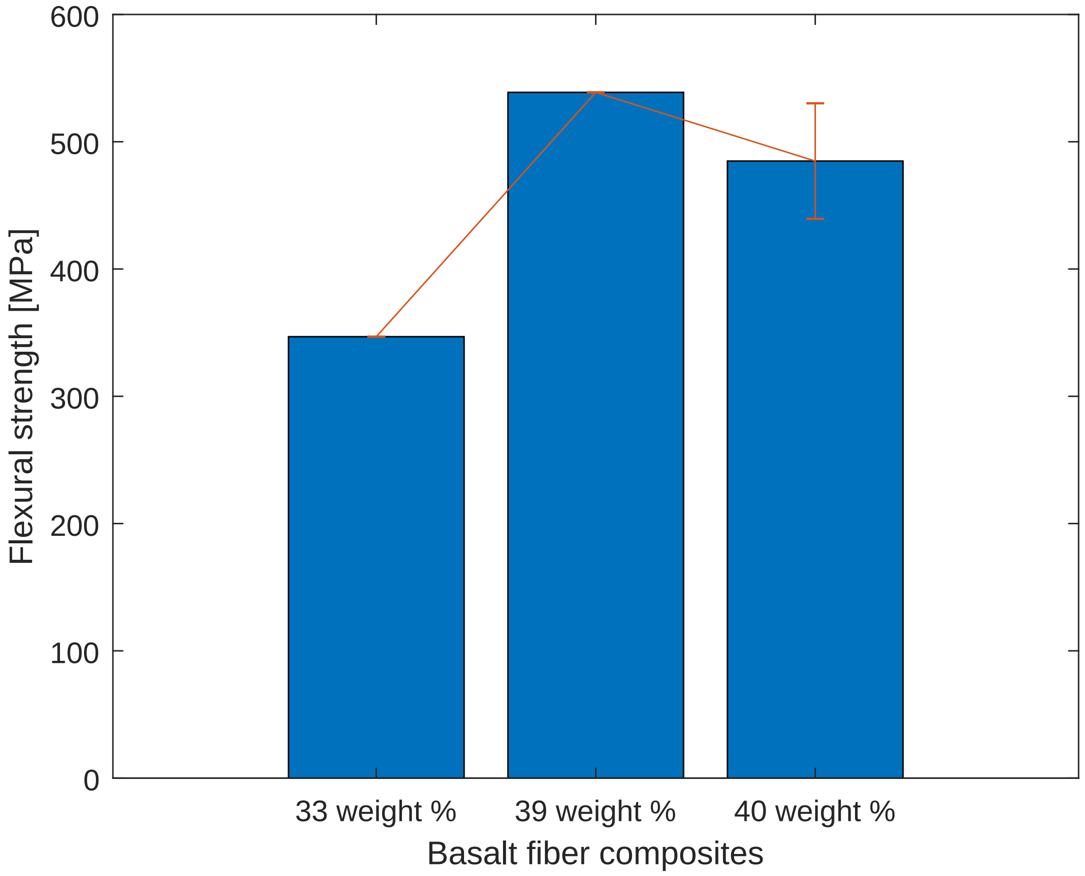

Figure 4.15 Flexural strength of basalt-reinforced composites with different fiber volume content.

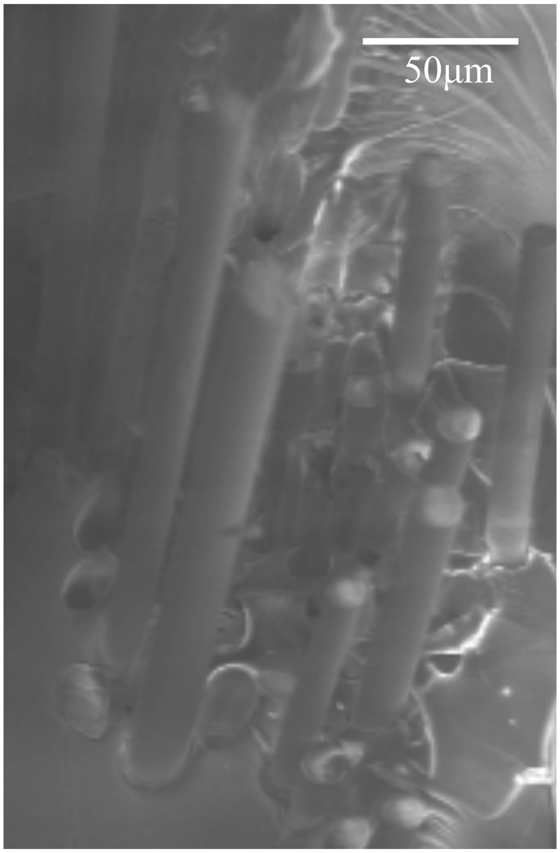

Figure 4.16 Fracture surface of basalt composite (40 weight %) showing almost no residues of resin on the surface of the fibers.

4.5.3 Fracture analysis

The single-fiber fragmentation tests revealed that the bonding strength between the basalt and the polymeric matrix was not high. This observation is also evident in the behavior of these fibers in the flexural tests conducted for the basalt-reinforced composites. As can be observed in figure 4.17, the presence of voids on the fracture surface of the specimen indicate a poor adhesion of the fibers with the epoxy. This means that the fibers have been pulled-out with low resistance. Furthermore, the surfaces of the basalt fibers show no signs of resin, an additional characteristic of poor fiber-matrix adhesion. Also, there are river patterns on the side of the fracture surface that was subjected to tension. This is a characteristic of high strength of the fiber, but low bonding strength between the filler and the matrix.[29].

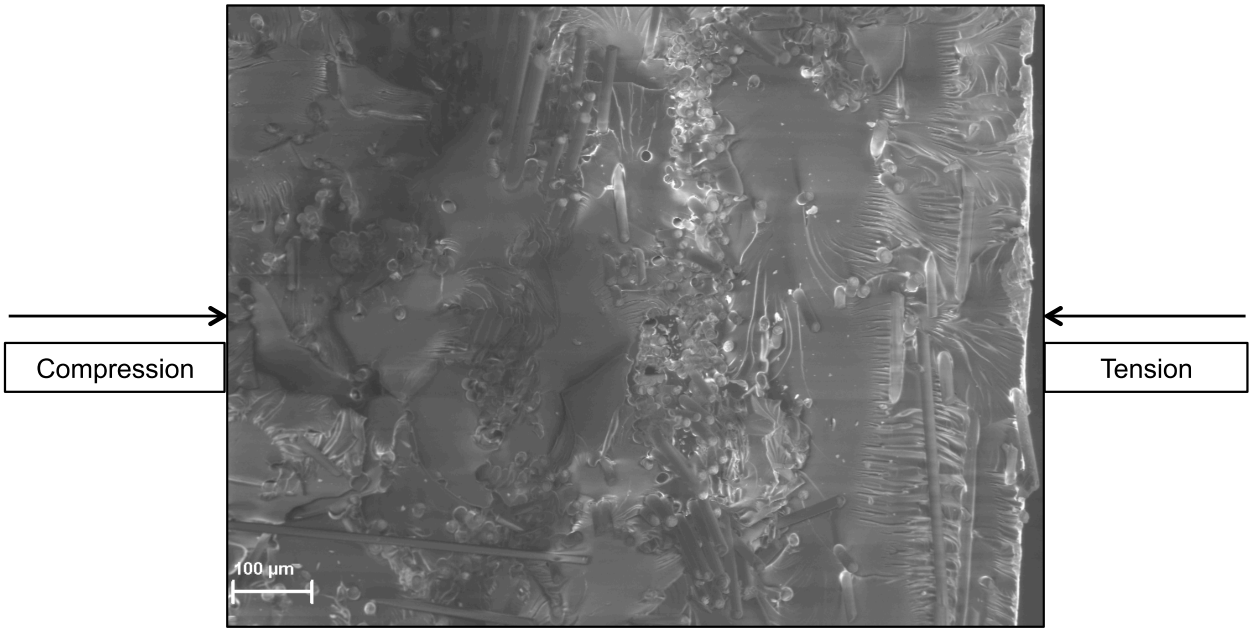

Figure 4.17 SEM micrograph of fracture surface of basalt composite (40 weight %) at the edge on the specimen subjected to compression.

Figure 4.18 shows the side of the fracture surface of a specimen subjected to a three point bending test. The area inside the circle shows a clear gap between the fiber and the matrix. This type of low-adhesion characteristics are sources for crack propagations. Also, this region demonstrates that a poor adhesion results in the formation of a layered fracture surface of the matrix[29].

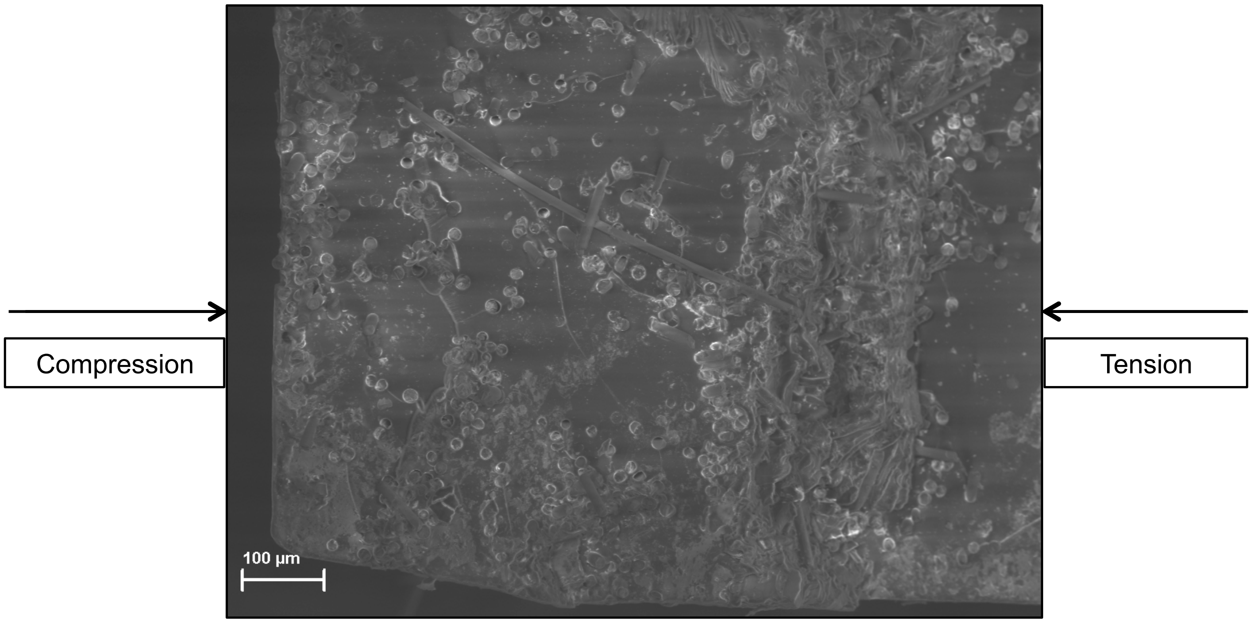

Figure 4.18 SEM micrograph of fracture surface of basalt composite (40 weight %) on the side of the tension edge.

Another important feature of the failure mode of the specimen is shown in figure 4.19, where the matrix surface on the right shows evidence of polymer debris, demonstrating tensile failure of the sample. This micrograph also shows that the fibers break at different lengths, suggesting that some energy absorption has taken place. This is an important feature of basalt fibers.

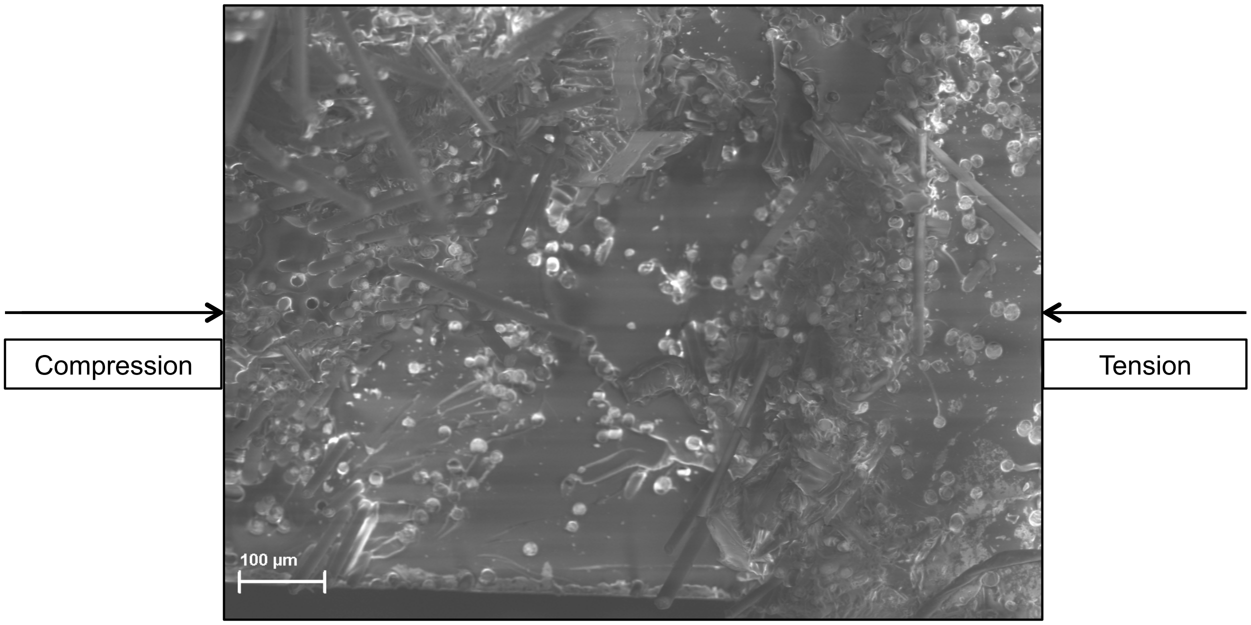

Figure 4.19 SEM micrograph of fracture surface of basalt composite (40 weight %) at the middle of the sample.Note mixture of failure modes.

4.6 Hybridized composites

4.6.1 Introduction

The specimens were prepared with the method reported in detail in section 4.2. The basalt and bamboo fibers were manually placed in the composite, such that the two types of fibers would be intermingled. This was achieved by alternating one toe of basalt fibers (approx. 400 fibers) with one AFEX-treated bamboo fiber. This type of distribution of fibers is regarded as *commingled*. In order to understand the synergetic effect of both types of fibers in the composite, this type of fiber arrangement was chosen. This randomization of the fiber distribution was divised to make a first assessment of the overall properties of the composites.For convinience, the weight fraction of basalt fibers will be denoted as $B_{w\%}$ and the AFEX-treated bamboo fiber weight fraction as $A_{w\%}$. Since the main goal of the present study is to develop high-performing composites, adding basalt fibers can be of great interest against the environmental degradation. It has been shown that the mixing of natural fibers with more durable fibers (such as basalt) can mean a higher resistance to aging effects of the composite[65]. [h]

Table 4.1 Conversion of weight to volume fraction of fibers in hybrid composites [a]

Sample weight percent ratio (AB/B) [b]	Bamboo fiber weight (%)	Basalt fiber weight (%)	Total fiber weight (%)	Bamboo fiber volume (%)	Basalt fiber volume (%)	Total fiber volume (%)
40/0	40	0	40	41	0	41
30/10	30	10	40	31	5	36
20/20	20	20	40	21	10	31
0/40	0	40	40	0	23	23

[a]: Conversion made with density for dry AFEX-bamboo fibers of $\left(1.1595\frac{g}{cm^3}\right)$ and basalt fiber density of $\left(2.6295\frac{g}{cm^3}\right)$. [b]: AB/B denotes weight ratio of AFEX-treated bamboo to basalt fibers

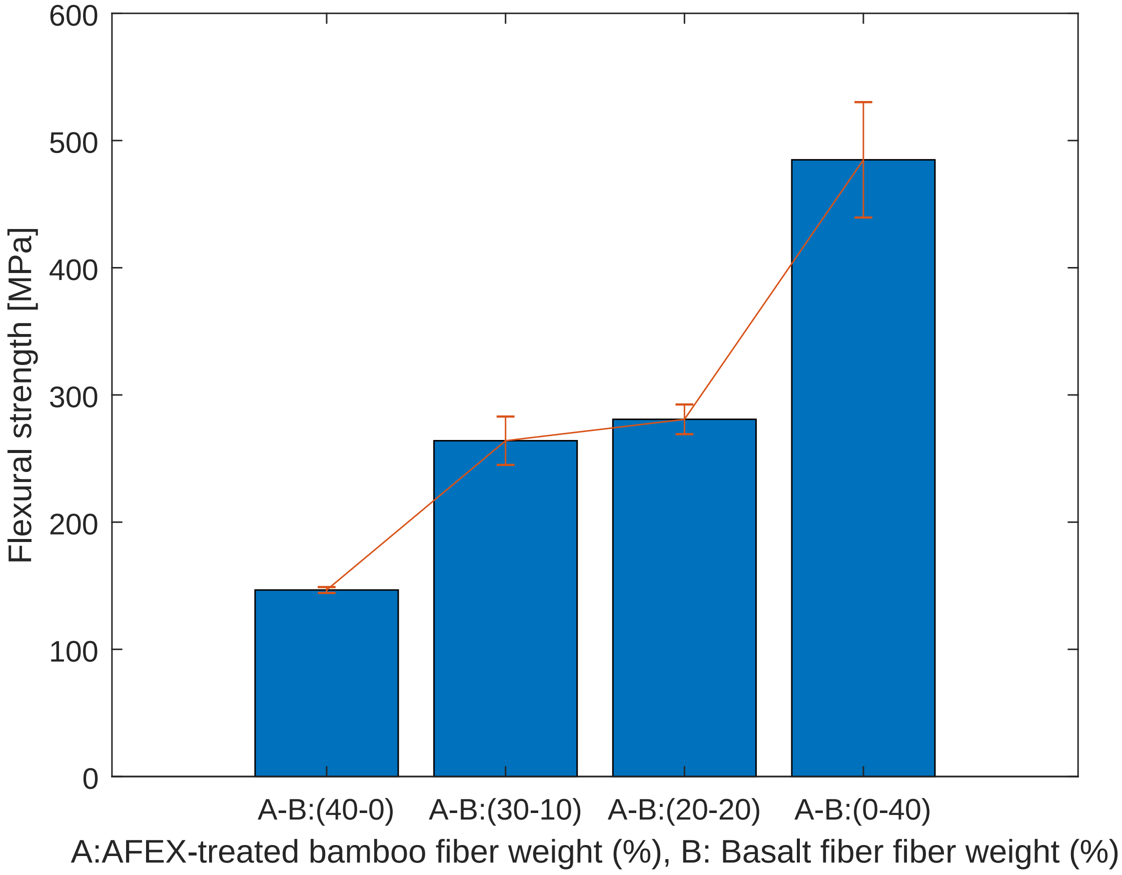

Figure 4.20 Flexural strength at different ratios of fiber weight percentage

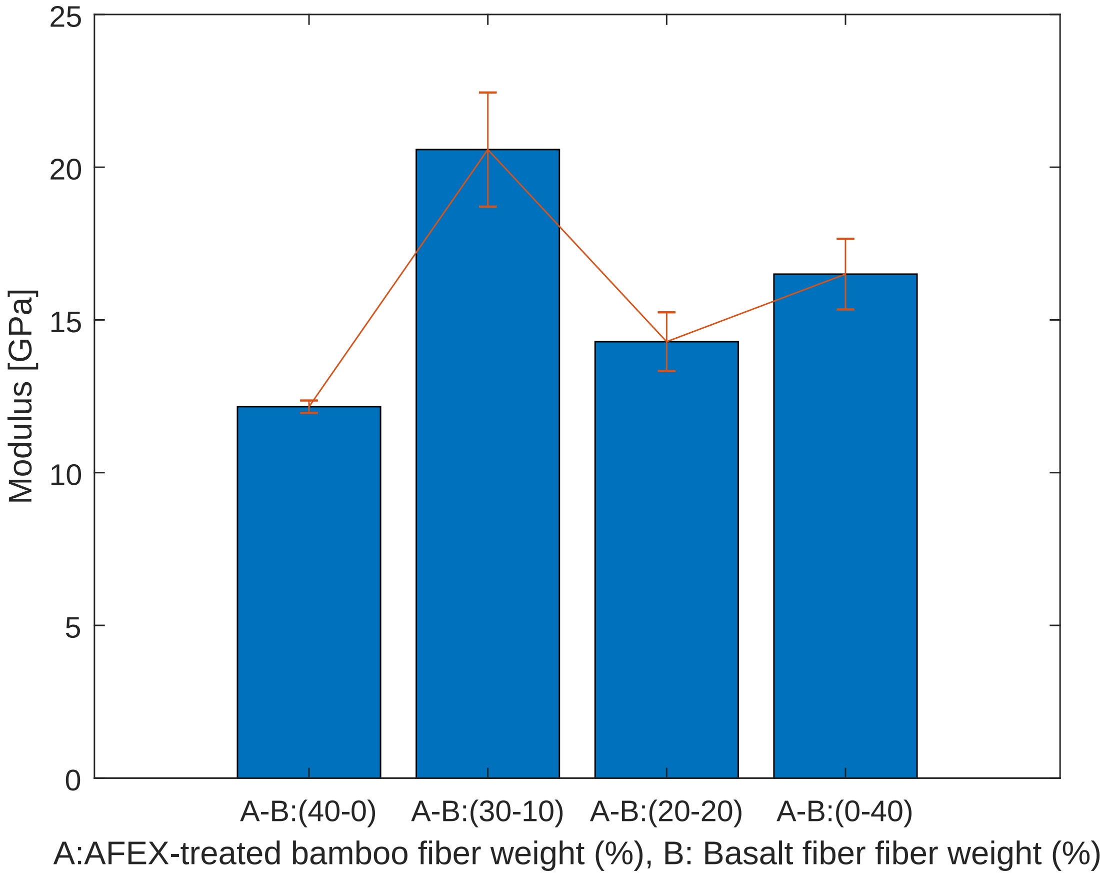

Figure 4.21 Flexural modulus at different ratios of fiber weight percentage

4.6.2 Fracture analysis

The following micrographs were taken in a scanning electron microscope (Model EVO-ZEISS, Germany) under variable pressure mode. This mode was selected in order to avoid charging of the non-conductive sample and therefore eliminate the need of coating. The following micrographs show the fracture modes on the surface of the samples subjected to three-point bending test.

4.6.2.1 Composites of $A_{w\%}$=20 and $B_{w\%}$=20

In figure 4.22 it is possible to observe a void formation around the bamboo-rich region. Towards the middle of the sample (on the left side of the figure) it is possible to identify a bundle of basalt fibers. This micrograph also demonstrates the break of bamboo fibers at different heights on the side subjected to tension, indicating energy absorption of the sample. Furthermore, it is possible to observe a crack almost perpendicular to the side of the sample on the side of tension, which may be an indication of delamination that increases the energy absoprtion amount of the composite.[28]. There are other features of interest on the fracture surface. One of them is the presence of river patterns as shown in the bottom left region of figure 4.23 as well as *hackles*. This resin-rich region demonstrates a tensile failure mode of the composite in the surroundings of bamboo fibers. A good adhesion between the bamboo fibers and the matrix is observed due to the breaks of the fibers (rather than pull-out features). This is not the case of basalt fibers in this hybrid composite as can be seen in figure 4.24. In the polymer region between the basalt and the bamboo fibers there is no sign of river patterns. Probably this is due to the poor bonding between the matrix and the basalt fibers. There are traces of crack formation pn the top right side of the figure, around the bamboo fibers. This is a remarkable characteristic of basalt fibers, since it hinders the micro-crack propagation, as compared to bamboo[1]. Nontheless, the poor adhesion of the basalt to the matrix

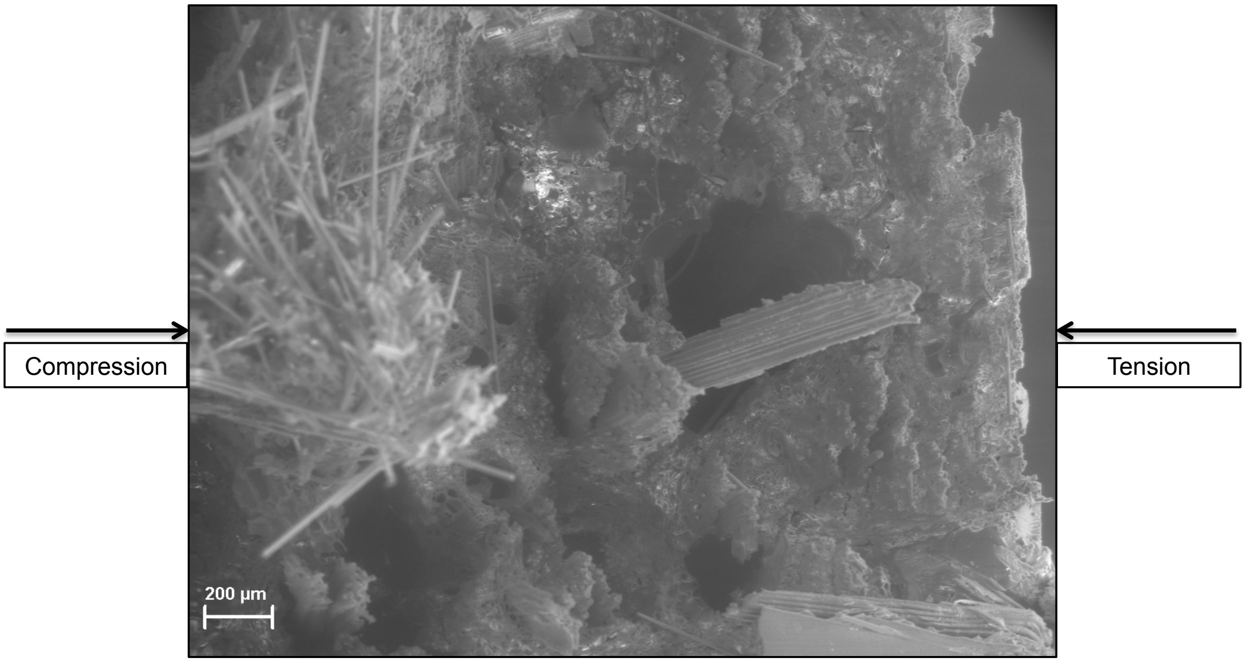

Figure 4.22 Fracture surface showing the edge of the sample subjected to tension. Note basalt fiber accumulation.

has a negative effect in the transfer of loads (see pulled-out fibers in the figures of section 4.5).

Figure 4.23 Hybrid composite 20%/20% AFEX/Basalt on tension edge. Bamboo fibers have failed by break. River patterns on resin surface.

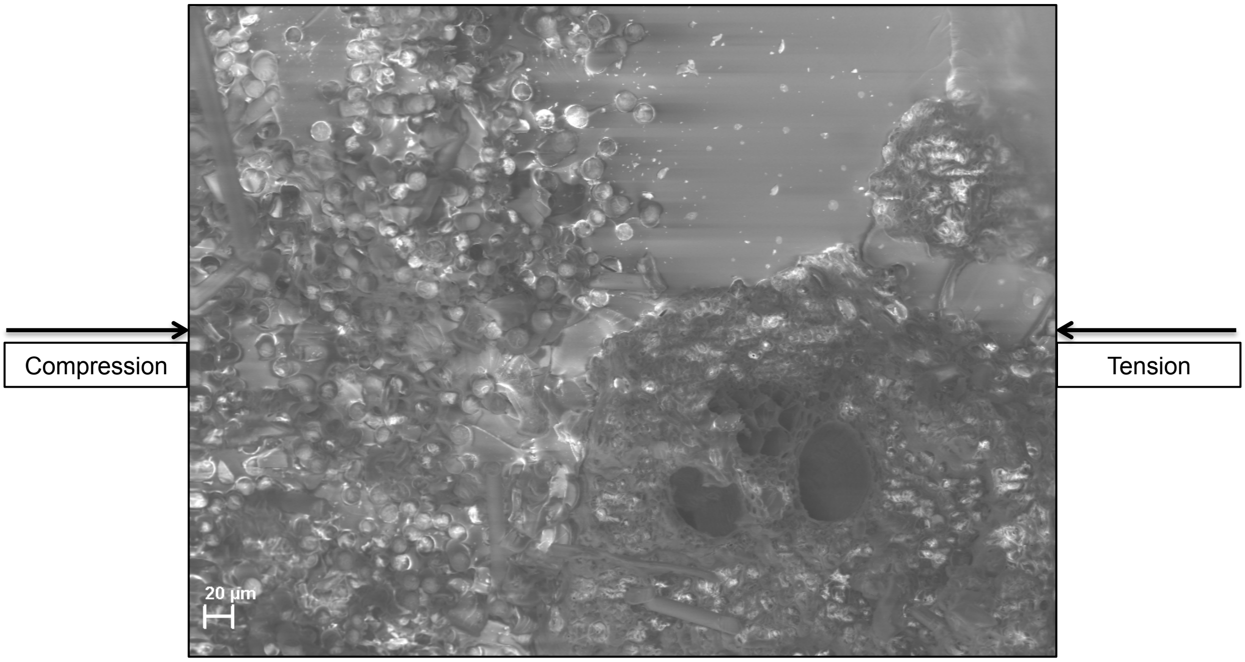

Figure 4.24 Hybrid composite 30%/10% AFEX/Basalt in the center of sample. Crack propagation around the bamboo fiber bundle. Basalt fiber pulled-out.

4.6.2.2 Composites of $A_{w\%}$=30 and $B_{w\%}$=10

[h] In this section, the fracture surfaces of composites containing 30 percent in weight of bamboo fibers (AFEX-treated) and 10 percent in weight of basalt are analyzed. This composition shows the highest value of modulus (see figure 4.21). This can be explained by observing the basalt composites and the bamboo composites. Since the bonding of bamboo with the epoxy matrix is high, the load can be transferred to these fibers in the composites. However, the bamboo fibers are prone to crack propagation (as can be seen in figures 4.22 and 4.23). On the other hand, basalt fibers are not very well adhered to the matrix but they show no signs of micro-crack propagation in the vicinity of the fiber bundles. Therefore, the combination of both types of fibers create a positive effect in the overall modulus of the composite (see 4.21). This effect is evident in figure 4.25 where the matrix has undergone a great amount of deformation close to the bamboo fibers. Also in the same figure, there is a formation of cracks on the left side of the micrograph, in a region of bamboo predominance. This hypothesis is again confirmed in 4.27 where the resin surface is almost undistorted (left side of the micrograph, close to the basalt fibers) while the right side of the figures shows delamination along the bamboo fibers and traces of cracks. It appears that the ratio of 30/10 weight percent of bamboo to basalt yields the highest stiffness of the composites. However, for the case of strength, the hybridization does not seem to not have this synergetic effect. This might occur because the strength of the composite is strongly dependant on the fiber properties. Specially in the case of three-point-bending tests, the mechanisms of As a result of the increased glass fibre content, the flexural strength increases with the addition of basalt fibers because of the higher shearing resistance[47]. A similar result is found in the study conducted by Sreekala et al[62], where the flexural strength of the hybrid composites increases with glass-fiber content, while the modulus decreases. The authors argue that, in a hybrid composite system, the fiber with the smallest elongation at break will determine the strength. This is also observed in the present study.

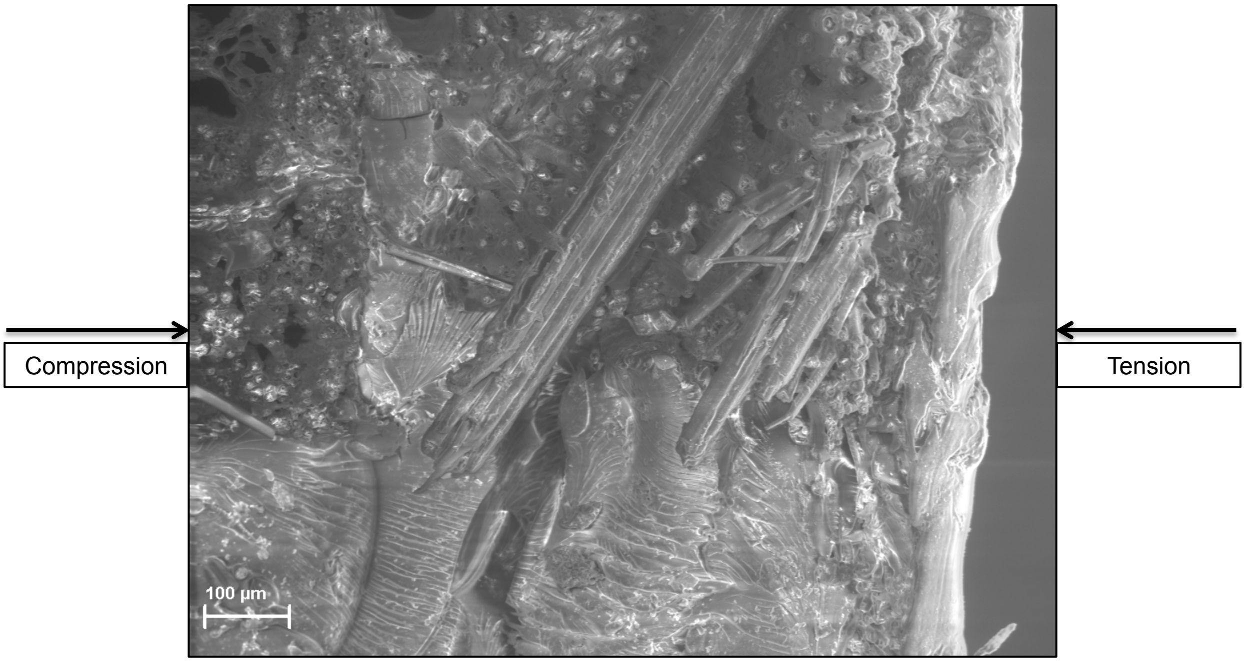

Figure 4.25 Hybrid composite 30%/10% AFEX/Basalt on tension edge. Note matrix deformation and voids formed

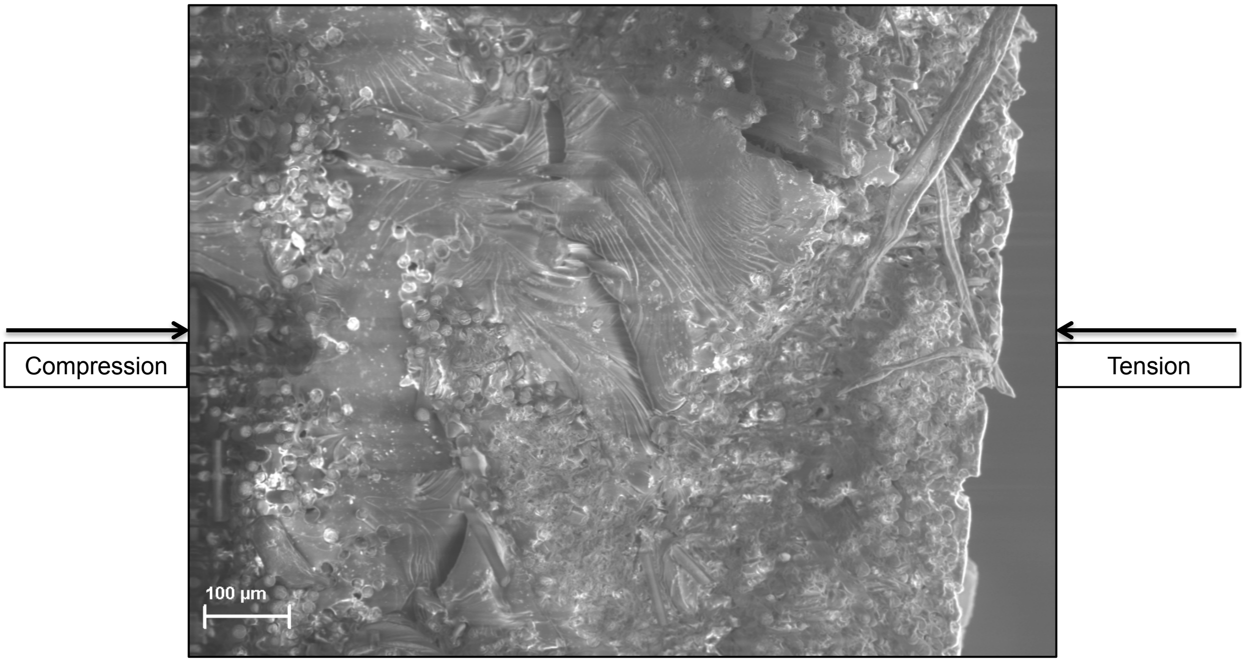

Figure 4.26 Hybrid composite 30%/10% AFEX/Basalt on tension side. Note resin-rich region and basalt fibers pulled out.

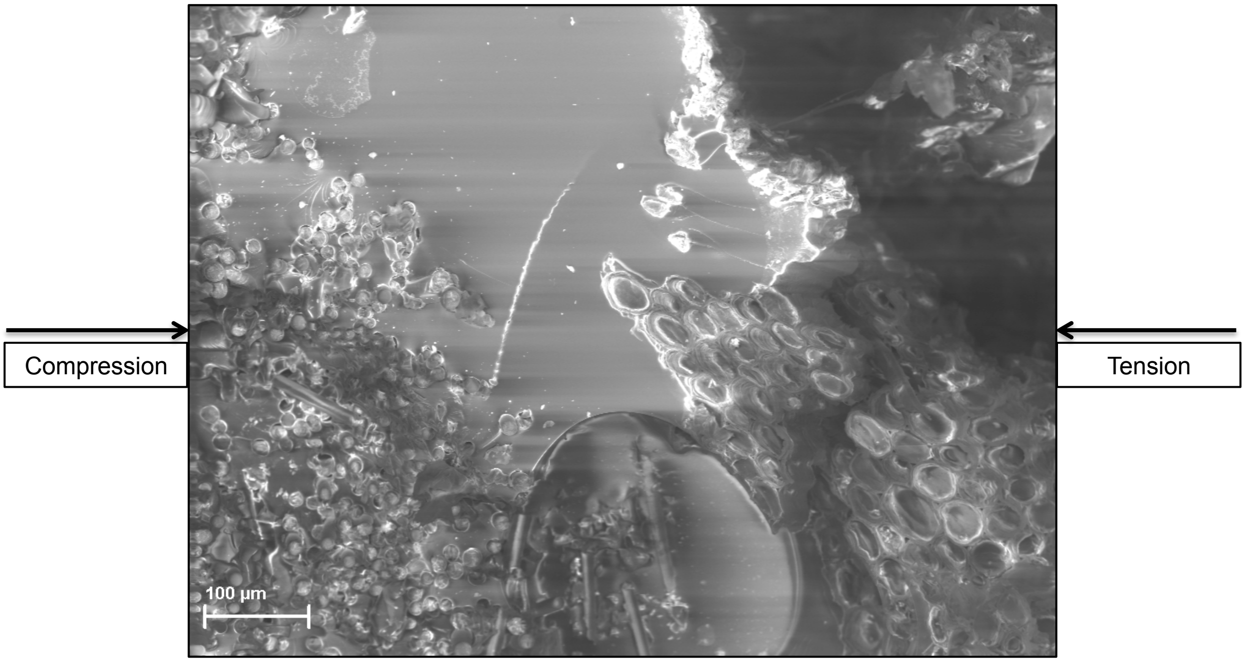

Figure 4.27 Hybrid composite 30%/10% AFEX/Basalt in center of the sample. Failure by delamination on the right side. No deformation of resin region.

4.6.3 Rule of mixtures

The rule of mixtures (*ROM*) is a mathematical tool to compute the properties of a composite, based on the weighted average of the fiber volume fraction. The rule of mixtures, in its ideal case, assumes no porosity[4]. Mathematically, the rule of mixture for composites with one type of fiber is expressed as:

$$X_c = fX_f + (1-f)X_m \tag{4.3}$$

where f is the volume fraction and X denotes the property. This could be density, flexural modulus, flexural strength, to name a few. The terms $\mathrm{X_c}$, $\mathrm{X_f}$, and $\mathrm{X_m}$, represent the property of the composite, the fiber, and the matrix, respectively. Since bamboo fibers vary considerably in volume, the weight of the fibers were measured for the fabrication of composites to make a reproduceable method. For this reason, there is the need to convert from weight fraction of fibers in the composite (w) to volume fraction (f). This is done with the ROM for densities (ρ_z), where the subscript z is f,m, and z for the fibers, the matrix, or the composite. If in the following equation

$$\rho_c = f\rho_f + (1-f)\rho_m \tag{4.4}$$

f is expressed as:

$$f = \frac{V_f}{V_f + V_m} \tag{4.5}$$

where $V_f + V_m$ is the total volume, or the volume of the composite, defined as V_c. With the definition of density ρ, as

$$rho = \frac{m}{V} \tag{4.6}$$

and

$$w \equiv \frac{\rho_f V_f}{\rho_f V_f + \rho_m V_m} \tag{4.7}$$

the volume fraction of fibers are calculated by:

$$f = \frac{1}{\frac{\rho_f}{\rho_m}\left(\frac{1}{w} - 1\right) + 1} \tag{4.8}$$

For the calculation of hybrid composites, the ROM has to be slightly modified, as follows:

$$X_c = f\,(AX_A + BX_B) + (1-f)X_m \tag{4.9}$$

where A and B are the fraction coefficients for bamboo and basalt, respectively. X_A and X_B are the properties for bamboo and basalt, respectively. Furthermore, the following equation holds always true:

$$A + B = 1 \tag{4.10}$$

Using the ROM for the results for flexural strength and modulus for bamboo and basalt composites, shown in sections 4.5 and 4.4, respectively, the following properties are obtained: Using the results

Table 4.2 Flexural strength and modulus calculated for basalt and bamboo fibers using ROM [a]

Fiber	**Strength in MPa (SE)**	**Modulus in GPa (SE)**
Bamboo	264.65 (22.145)	29.896 (2.0462)
Basalt	1769.5 (153.49)	59.3402 (3.2419)

from table 4.2 as the expected values for the modulus and strength of bamboo and basalt fibers, and the nominal flexural properties for the matrix indicated in chapter 1, the following plot was generated:

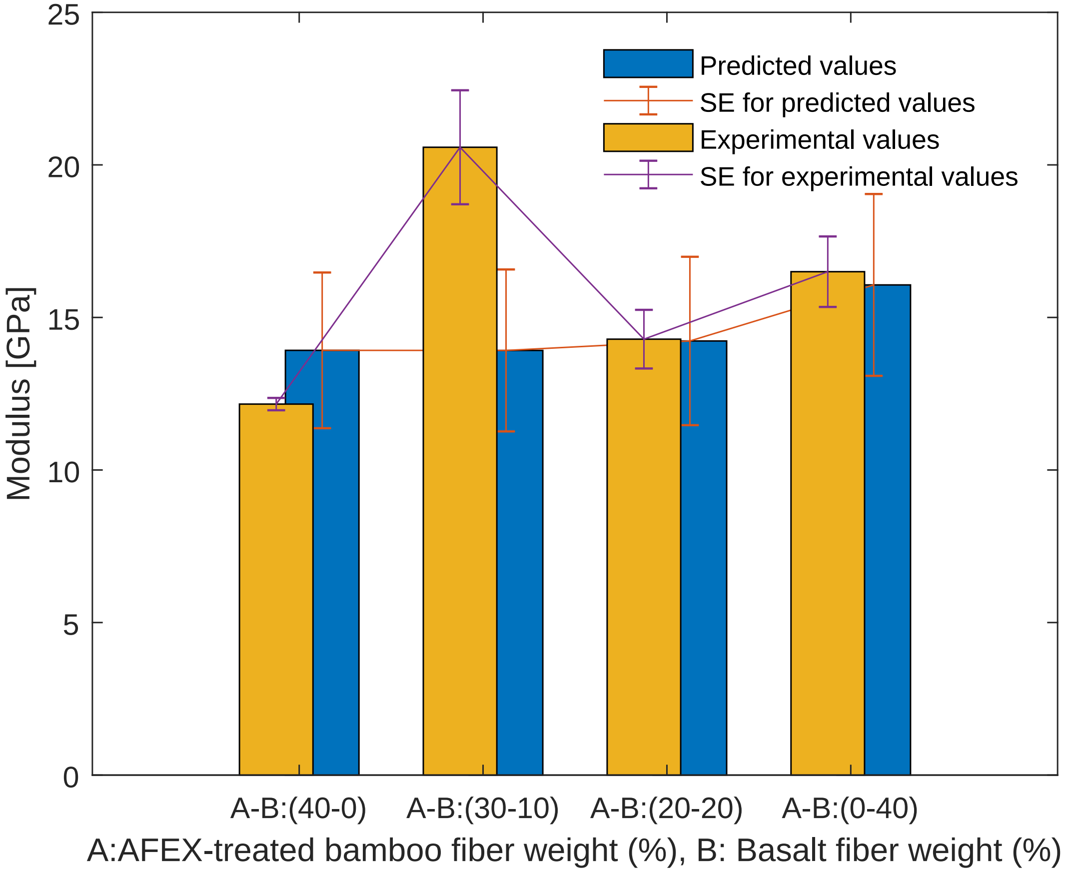

Figure 4.28 Flexural modulus comparison between predicted and calculated values in hybrid composites

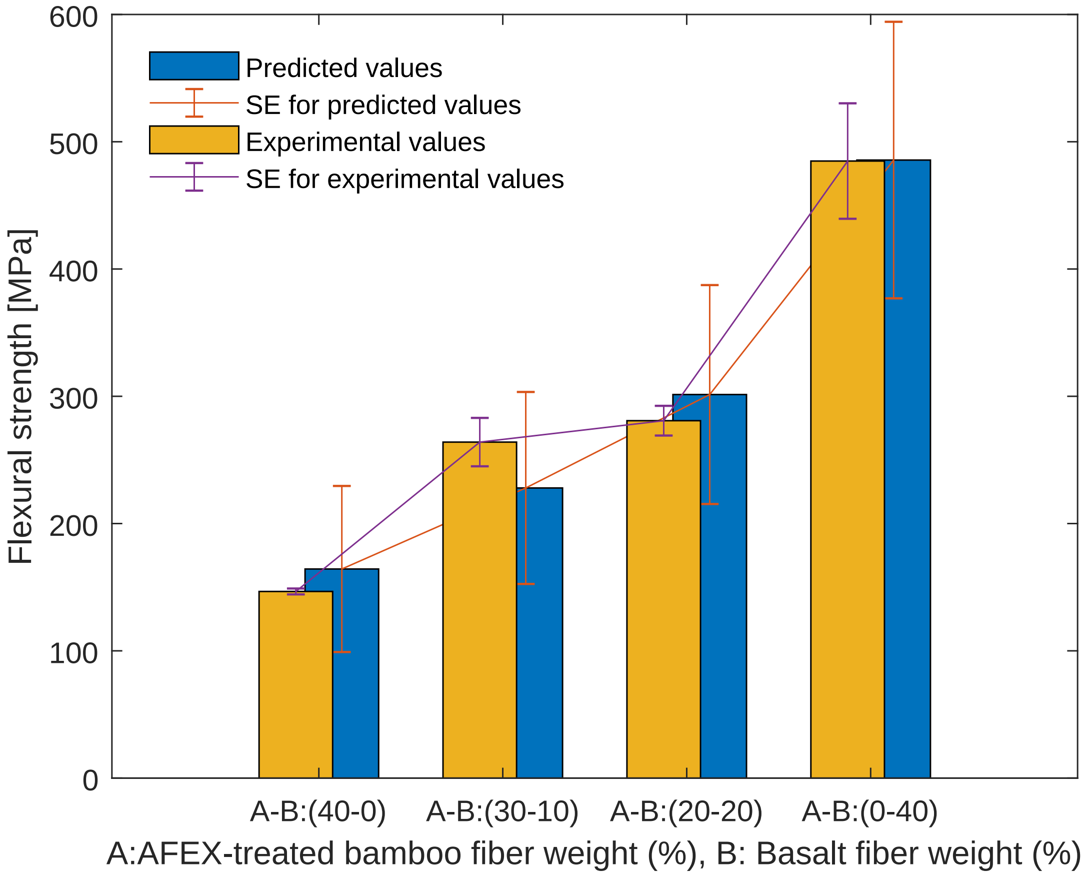

Figure 4.29 Strength comparison between expected and observed values.

It is remarkable to observe the behavior of the hybrid composite at 30 weight percent bamboo with 10 weight percent in terms of the modulus (see figure 4.28). That is the synergistic effect that yields a modulus higher than predicted by ROM[37]. It would be necessary to conduct more experiments to study this phenomenon in depth. For the case of figure 4.29, the predicted values are in good agreement with the experimental ones. It is worth noting that the values taken for the fiber modulus and strength are the average and do not include the standard deviation.

CHAPTER 5

CONCLUSIONS AND FUTURE WORK

5.1 Mechanical behavior of composites

The present study has shown that the it is possible to achieve good flexural properties of bamboo/basalt hybrid composites in an epoxy resin. Furthermore, the synergetic effect of the combination of these two types of fibers is presented. It has been shown that the flexural modulus is increased by approximately 66%. Additionally, the failure characteristics were investigated in order to understand the mechanisms involved and, ultimately, determine ways to improve the quality of the composites.

Since the bamboo and the basalt fibers possess different physical and mechanical features, a series of tests were conducted to maximize their performance in the composite. The AFEX treatment was proven to be an effective, and environmentally-friendly way to process the bamboo fibers. This treatment reuses up to 99% of the original ammonia, which conversely produces significant waste. The bamboo fiber-bundles obtained show good adhesion to the matrix due to their shared hydrophilicity character. The surface roughness of AFEX-bamboo is greater than other fibers, which also adds to the good mechanical properties observed in the composites.

The TGA on the AFEX-bamboo revealed that the hemi-cellulose and the lignin present were reduced. This is important to a certain degree because the fiber bundles are left with more suitable components (such as a greater degree of cellulose) for structural features. Although the water uptake of water after the AFEX treatment was still high, the water desorption is quickier. This is of particular interest for the industry, since it means shorter times of drying, less energy, and therefore, cost reductions.

In the case of basalt fibers, they did not undergo any treatment for the composite fabrication. As the TGA figure shows, their water absorption is very small, as well as the degradation up to 600ºC. Although the strength of the hybrid composites increased with the weight content of these fibers, the single fiber fragmentation and SEM fracture surface show a poor bonding strength with the epoxy.

In terms of the fabrication process of flexural coupons, a simple method was developed, that yielded good wetting of the basalt and bamboo fibers and a minimal void content. An important aspect of this technique is that it does not require mechanical pressure or vacuum. This is translated into a reliable, easily reproduceable fabrication technique to make composites. This resin-pouring method also assures a high degree of alignment and dispersion of the fibers, which is vital for high-quality unidirectional coupons.

The SEM micrographs revealed that the failure mechanisms are different depending on the filler used (basalt, bamboo, or hybrid fillers). In the case of bamboo, the bonding strength to the matrix caused the flexural samples to form hackles and river patterns on the surface of the epoxy. Also, the fibers broke at different heights, which is an indication of energy absorption by the system. This characteristic is desireable in many structural and impact applications. In the case of basalt composites the low adhesion of the fibers to the epoxy caused pull-outs of the fibers from the matrix. This needs to be improved in order to utilize the intrisic mechanical properties of the fiber. Basalt fibers are remarkable for the amount of energy they can absorb, which is why, partially, the matrix in the vicinity of the fibers of the fracture surface show no matrix distortion. This characteristic can be advantageous to avoid the micro-crack propagation and therefore, create stronger composites.

5.1.1 Bamboo fiber performance

The AFEX treatment conducted on the bamboo culms proved to be positive as a harvesting technique. After this pretreatment, the fiber bundles were easy to harvest without applying mechanical pressure with a rolling-mill. The rolling-mill could deteriorate the cristallinity of the fibers and create defects that possibly derive in lower strength. Moreover, thys type of fiber displayed good adhesion with the epoxy matrix. In order to improve the performance of the fibers, the parameters of the AFEX treatment can be studied. These parameters include the pH, the time of treatment and the temperature. This procedure would allow to find the ideal hemicellulose and lignin content.

Additionally, fibers of smaller diameter could result in higher mechanical properties[52].

5.1.2 Basalt fiber performance

A good adhesion is crucial to the performance of the composite, and therefore there is the imperative need to find surface treatments for the basalt fibers. In this study, it has been that the basalt fibers did not ehxibit epoxy residues on their surfaces. This poor bonding strength also derived in fiber pull-outs, which is detrimental to the overall performance of the composite. One important feature of the AFEX treated fibers is the increase of surface roughness compared to the ones harvested with the pressure chamber. It is hypothesized that this surface characteristic is translated into mechanical locking to the matrix which, in turn, creates a higher flexural modulus to the composites.

5.2 Next steps

5.2.1 Sizing of basalt fibers

As mentioned before, the poor interfacial bonding between basalt and epoxy is detrimental for the composite performance as a whole. There are several ways to increase the adhesion of these fibers with the epoxy matrix. The nano-hybrid of silicon dioxide (SiO_2) with epoxy as one candidate to increase the bonding strength with the matrix and, consequently, increasing the strength of the composite[68]. Another coupling agent for this purpose is *silane*. Silanes are covalently-bonded compounds of silicon and hydrogen in the form: Si_nH_{2n+2}. This is a very versatile compatibilizer that can be used in different matrices. Mafic basalt fibers, among other companies, offer silane-treated, continuous fibers, compatible for different polymeric matrices, such as polypropylene, epoxy, vinyl ester, polyurethane, and polyamides (PET/PBT)[42]. The effectiveness of silane treatments for the enhancement of flexural strength is attributed to the change in the pH of ionic silane compounds when combined with the fibers[64].

5.2.2 Fiber distribution for improvement of flexural properties

In this work, the basalt and bamboo fibers were distributed randomly in the composite. However, a more rational approach in order to increase the modulus is to place the stiffer fibers (i.e. basalt) as far as possible from the neutral axis in the three point bending test. For this purpose, instead of fabricating single lamina of hybrid composites, a laminate structure could be prepared. The fabrication of one-fiber-type composites yields better control of the dispersion of fibers. After the preparation of the laminae, they would be stacked in a sequence to form a laminate. A *sandwich* arrangement for the laminate is desireable, where the laminae of basalt-reinforced composites lie away from the neutral axis[37].

5.2.3 Impact tests

As the fracture surfaces of this study suggest, the energy absoprtion of the hybrid composites is high even for the low adhesion strength of basalt with epoxy. The lack of crack propagation in the environment of basalt fibers suggest that the here-studied composites can take an important amount of energy before failing. To determine this hypothesis, the composites can be tested in Izod impact tests. Furthermore, the behavior of the energy uptake of the materials can be assessed as a function of the environment, by varying the temperature and humidity of the composites. Furthermore, the change of the environment conditions of the tests could verify the claim that basalt fibers have superior properties in terms of their dimensional stability when compared to glass fibers.

APPENDICES

APPENDIX A

MATLAB CODE FOR THERMOGRAVIMETRIC ANALYSIS

```
clc
close all
clear all
filename = 'not dried sample.txt';
A = importdata(filename);
%A = xlsread(filename);
deriv = A(:,3);
T = A(:,1);
fig=figure;
Distance=500;
[peaks, locations] = findpeaks(deriv,'MinPeakHeight',0.2,'MinPeakDistance',Distance);
hold on
%Temp=T(locations)
%Derivative=peaks
%[pks, locs]= findpeaks(locations,peaks,'Annotate','extents','MinPeakHeight',0.5);
a=plot(T,deriv);
%scatter(T(locations),deriv(locations),40,'filled')
scatter(T(locations),peaks)
n=length(peaks);
i=1;
%horizontal=0*ones(length(T));
%plot(T,horizontal)
```

```
Temp=T(locations);
Pks=peaks;
while i<=n
Temperature=Temp(i)*ones(length(Pks));
Height=0:Pks(i)/(length(Temperature)-1):Pks(i);
        plot(Temperature,Height,'--')
        text(Temperature(i),Pks(i),int2str(Temp(i)),'HorizontalAlignment','center','VerticalAlignment','bottom')
        i=i+1;
end
%plot(plot
%deriv(pks)
hold off
xlim([25 500])
ylim([0 1])
ylabel('Weight loss (%/C)')
xlabel('Tempertature (C)')
grid
legend(a,'Not dried AFEX bamboo')
fig.PaperPositionMode = 'auto';
fig_pos = fig.PaperPosition;
fig.PaperSize = [fig_pos(3) fig_pos(4)];
saveas(fig,'\\tsclient\home\THESIS DOCUMENT\images\notdriedAFEX.pdf')
```

```
%save('\\tsclient\home\THESIS DOCUMENT\images\
    notdriedAFEX.pdf')
```

APPENDIX B

ESTIMATION OF FIBER VOLUME FRACTION IN COMPOSITES WITH IMAGEJ

Motivation : Due to the inherent variability of the the dimensions and density of natural fibers, the assumption of a cylindrical shape can yield erroneous calculations of the volume fraction present in the fibers. Therefore, a first attempt to estimate the volume fraction is presented in this section.

Procedure : The bamboo-reinforced composites were polished using the procedure described in section 4.3. Then, the samples were observed under the light transmission microscope (Keyence, USA). The optical microscope needs to be calibrated and each micrograph should show a scalebar. The images were saved as *tiff* (Tag Image File Format) files for evaluation with the ImageJ software[56]. The micrographs were evaluated using the following procedure:

- Open the desired file. Command: `File→ Open...`
- Improve contrast. Command: `Process → Enhance contrast`
- Convert image to scale of grey image type: `Command Image → Type → 8bit`
- Filter out wavelength of the image that correspond to the matrix. Command: `Image → Adjust → Threshold`. The value for the threshold varies from sample to sample. The user has to find the right setting to have adequate results.
- Convert image to black and white image. Command: `Process → Binary → Make binary`
- Select option to measure area. Command: `Analyze → Set measurements... → Select Area checkbox`

- Calculate area (in units of pixels). Command: `Analyze` → `Measure`. This last step will return the total dark area of the image. The total dark area of the image, that corresponds to the fiber regions, is obtained by dividing this value to the total area of the image (shown at the top left side of the image).
- Generate negative image. Command: `Image` → `Lookup Table` → `Invert LUT`.
- Repeat *area measure* command. Compute area by dividing the value returned by the software by the total area of the image (in pixels).
- By adding the two area measurements, the area fraction of the bamboo region is computed.

Although the aforementioned procedure is straightforward, there is not one single recipe for all samples since the contrast changes. Therefore it is advised to adjust the optical parameters in ImageJ accordingly. This is specially important for composites where the contrast between the matrix and the bamboo fibers is low. This technique is not necessary for synthetic fibers because they are posses less variations in their diameter, shapes. Thus, in the case of basalt, the main use of this procedure is to observe the fiber distribution. Also, the measurements for several cross-sections of the same sample should be done in order to better estimate the actual volume fraction. (see Table 5.1).

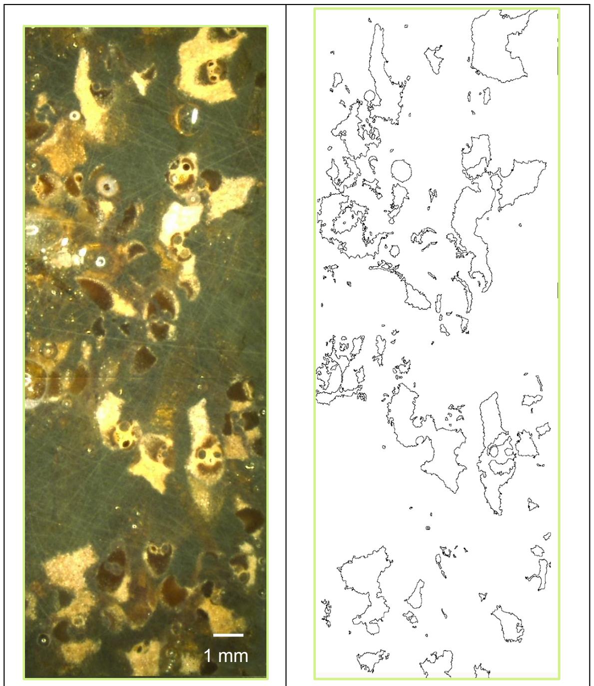

Original image Bright-bamboo area

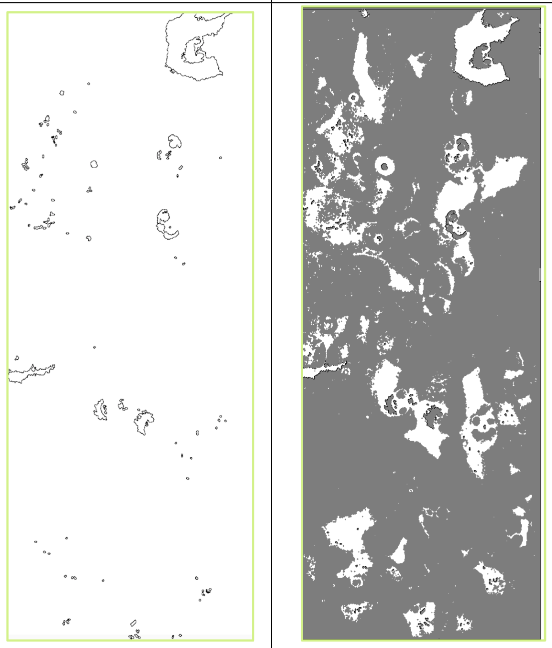

Dark-bamboo area Total area of bamboo

Figure 5.1 Example for the estimation of fiber volume by using ImageJ

Table 5.1 Example of bamboo-reinforced composite (AFEX-treated)

Sample	**Count**	**Total area (in pixels^2)**	**Average area size in pixels^2**	**Area (%)**
Sample 1 - Cross section 1	164	98844	602.707	14.993
Sample 1 - Cross section 2	169	99891	591.071	15.015
Sample 1 - Cross section 3	130	104381	802.931	15.492
Sample 1 - Cross section 4	295	106140	359.797	15.417
Sample 1 - Cross section Average	-	-	-	15.229 (SD=0.262)

APPENDIX C

BIODEGRADABLE POLYMERS AS MATRIX

The ultimate goal of this study is to promote the fabrication of high-performance composites with environmental sustainability. For this purpose, the study of the environmentally-friendly resins should be conducted. BASF has developed a series of acrylic resins that show interesting binding properties where the byproduct of the curing process is water. The reports of this product state that the cross-linking is achieved by the reaction of polycarboxylic acids with multifunctional alcohols. The only by-product caused by curing is water[7]. In a first attempt to characterize this product, a series of curing processes were conducted during this work. The neat resins exhibited a foam-like structure after curing (see figure 5.2, making them very difficult to test them for their mechanical aspects. The curing process for this sample was: 80ºC for two hours in a convection oven followed by a temperature rate of 10ºC/min to 160ºC. The temperature was held at 160ºC for 20 minutes.

The compression-moulded composite fabrication with AFEX-treated yielded better results, as shown in figure 5.3. For this specimen, a beaker with the 950L resin was heated for one hour at 80ºC. After this time, the resin was poured into a pre-heated mold at 160ºC and pressure of approx. 100lb was applied for 20 minutes. The system was allowed to cure naturally.

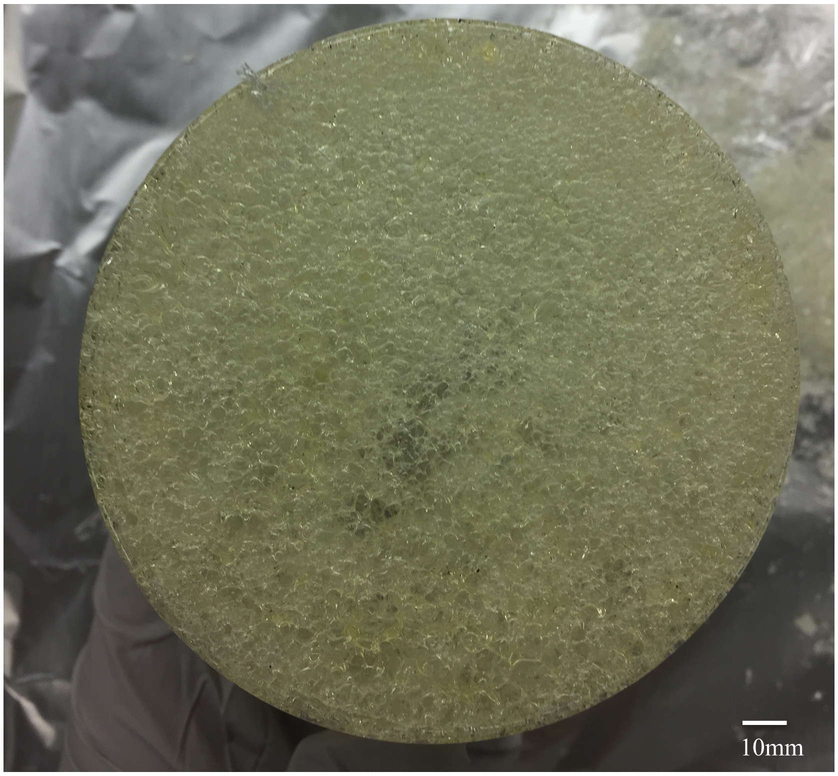

Figure 5.2 Foam structure of neat Acrodur 950L (BASF).

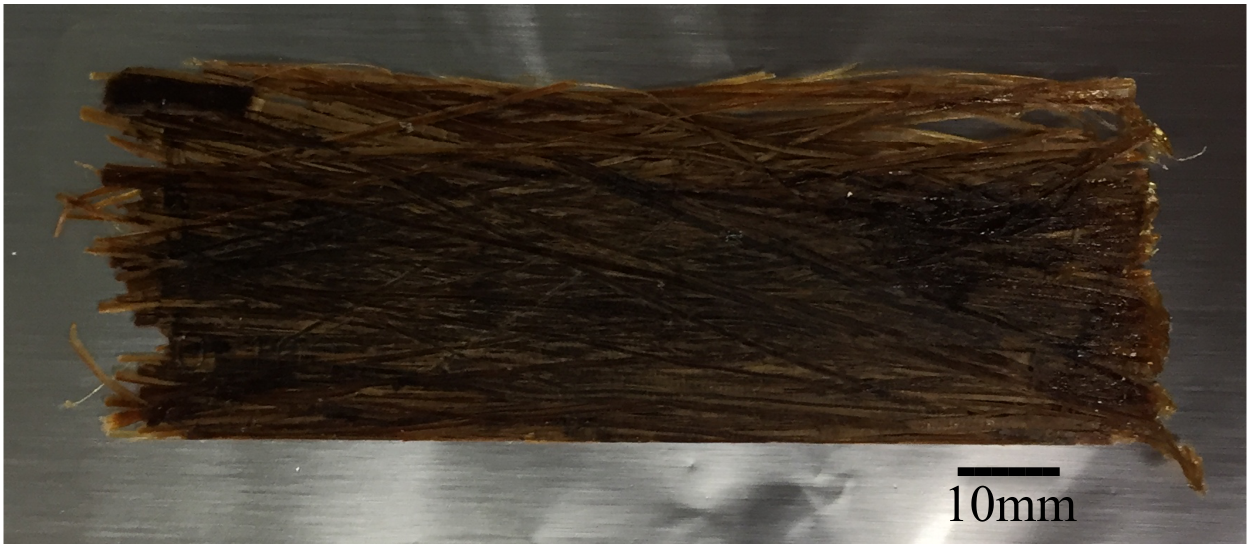

Figure 5.3 Compression-moulded Acrodur-950L (BASF) resin with AFEX-treated bamboo fibers.

BIBLIOGRAPHY

BIBLIOGRAPHY

[1] Agarwal, B. D., Broutman, L. J., and Chandrashekhara, K. (2017). *Analysis and performance of fiber composites*. John Wiley & Sons.

[2] Akinlabi, E. T., Anane-Fenin, K., and Akwada, D. R. (2017). *Bamboo: The Multipurpose Plant*. Springer.

[3] Amada, S. and Untao, S. (2001). Fracture properties of bamboo. *Composites Part B: Engineering*, 32(5):451–459.

[4] Ashby, M. and Bréchet, Y. (2003). Designing hybrid materials. *Acta materialia*, 51(19):5801–5821.

[5] Balasubramanian, M. (2013). *Composite materials and processing*. CRC press.

[6] Basaltex (2015). Basalt products. http://www.basaltex.com/en/detail_detail20_32.aspx. Accessed: 2018-03-30.

[7] BASF (2017). Acrodur acrylic resins. https://www.basf.com/us/en/products-and-industries/General-Business-Topics/dispersions/Products/acrodur.html. Accessed: 2018-01-15.

[8] Bendat, J. S. and Piersol, A. G. (2011). *Random data: analysis and measurement procedures*, volume 729. John Wiley & Sons.

[9] Block, E. and Smith, P. A. (2018). Amine. https://www.britannica.com/science/amine. Accessed: 2018-03-30.

[10] Brik, V. B. (1997). Basalt fiber composite reinforcement for concrete. Technical report.

[11] Buschle-Diller, G., Fanter, C., and Loth, F. (1999). Structural changes in hemp fibers as a result of enzymatic hydrolysis with mixed enzyme systems. *Textile research journal*, 69(4):244–251.

[12] Carlsson, L. A., Adams, D. F., and Pipes, R. B. (2002). *Experimental characterization of advanced composite materials*. CRC press.

[13] Carrillo, F., Colom, X., Sunol, J., and Saurina, J. (2004). Structural ftir analysis and thermal characterisation of lyocell and viscose-type fibres. *European Polymer Journal*, 40(9):2229–2234.

[14] Deák, T. and Czigány, T. (2009). Chemical composition and mechanical properties of basalt and glass fibers: a comparison. *Textile Research Journal*, 79(7):645–651.

[15] Dhand, V., Mittal, G., Rhee, K. Y., Park, S.-J., and Hui, D. (2015). A short review on basalt fiber reinforced polymer composites. *Composites Part B: Engineering*, 73:166–180.

[16] Dixon, P., Ahvenainen, P., Aijazi, A., Chen, S., Lin, S., Augusciak, P., Borrega, M., Svedström, K., and Gibson, L. (2015). Comparison of the structure and flexural properties of moso, guadua and tre gai bamboo. *Construction and Building Materials*, 90:11–17.

[17] Dixon, P. G. and Gibson, L. J. (2014). The structure and mechanics of moso bamboo material. *Journal of the Royal Society Interface*, 11(99):20140321.

[18] Downey, M. A. and Drzal, L. T. (2014a). Toughening of aromatic epoxy polymers via aliphatic epoxy monomer addition: Optimized fiber-reinforced polymer composites for lightweighting. *SPE Automotive Composites Conference & Exhibition Troy, MI, USA*.

[19] Downey, M. A. and Drzal, L. T. (2014b). Toughening of aromatic epoxy via aliphatic epoxy copolymers. *Polymer*, 55(26):6658–6663.

[20] Drzal, L. T., Rich, M. J., and Lloyd, P. F. (1983). Adhesion of graphite fibers to epoxy matrices: I. the role of fiber surface treatment. *The Journal of Adhesion*, 16(1):1–30.

[21] Farris, S., Schaich, K. M., Liu, L., Piergiovanni, L., and Yam, K. L. (2009). Development of polyion-complex hydrogels as an alternative approach for the production of bio-based polymers for food packaging applications: a review. *Trends in food science & technology*, 20(8):316–332.

[22] Faruk, O., Bledzki, A. K., Fink, H.-P., and Sain, M. (2012). Biocomposites reinforced with natural fibers: 2000–2010. *Progress in polymer science*, 37(11):1552–1596.

[23] Gong, X., Arthur, J., and Penn, L. (2001). Strain rate effect in the single-fiber-fragmentation test. *Polymer composites*, 22(3):349–360.

[24] Gupta, V., Drzal, L., Adams, W., and Omlor, R. (1985a). An electron microscopic study of the morphology of cured epoxy resin. *Journal of materials science*, 20(10):3439–3452.

[25] Gupta, V., Drzal, L., Lee, C.-C., and Rich, M. (1985b). The temperature-dependence of some mechanical properties of a cured epoxy resin system. *Polymer Engineering & Science*, 25(13):812–823.

[26] Gupta, V., Drzal, L., and Rich, M. (1985c). The physical basis of moisture transport in a cured epoxy resin system. *Journal of Applied Polymer Science*, 30(11):4467–4493.

[27] Hao, L. and Yu, W. (2010). Evaluation of thermal protective performance of basalt fiber nonwoven fabrics. *Journal of thermal analysis and calorimetry*, 100(2):551–555.

[28] Hariharan, A. B. A. and Khalil, H. A. (2005). Lignocellulose-based hybrid bilayer laminate composite: Part i-studies on tensile and impact behavior of oil palm fiber-glass fiber-reinforced epoxy resin. *Journal of Composite Materials*, 39(8):663–684.

[29] Harish, S., Michael, D. P., Bensely, A., Lal, D. M., and Rajadurai, A. (2009). Mechanical property evaluation of natural fiber coir composite. *Materials characterization*, 60(1):44–49.

[30] Holtzapple, M. T., Jun, J.-H., Ashok, G., Patibandla, S. L., and Dale, B. E. (1991). The ammonia freeze explosion (afex) process. *Applied Biochemistry and Biotechnology*, 28(1):59–74.

[31] Hyer, M. W. (2009). *Stress analysis of fiber-reinforced composite materials*. DEStech Publications, Inc.

[32] Jain, S., Kumar, R., and Jindal, U. (1992). Mechanical behaviour of bamboo and bamboo composite. *Journal of Materials Science*, 27(17):4598–4604.

[33] Jamshaid, H. and Mishra, R. (2016). A green material from rock: basalt fiber–a review. *The Journal of The Textile Institute*, 107(7):923–937.

[34] Jones, R. M. (2014). *Mechanics of composite materials*. CRC press.

[35] Kelly, A. and Tyson, a. W. (1965). Tensile properties of fibre-reinforced metals: copper/tungsten and copper/molybdenum. *Journal of the Mechanics and Physics of Solids*, 13(6):329–350.

[36] Kim, B. W. and Nairn, J. A. (2002). Observations of fiber fracture and interfacial debonding phenomena using the fragmentation test in single fiber composites. *Journal of Composite Materials*, 36(15):1825–1858.

[37] Kretsis, G. (1987). A review of the tensile, compressive, flexural and shear properties of hybrid fibre-reinforced plastics. *Composites*, 18(1):13–23.

[38] Kutz, M. (2015). *Mechanical Engineers' Handbook, Volume 1: Materials and Engineering Mechanics*. John Wiley & Sons.

[39] Lee, J. and Drzal, L. T. (2005). Surface characterization and adhesion of carbon fibers to epoxy and polycarbonate. *International journal of adhesion and adhesives*, 25(5):389–394.

[40] Liu, Q., Shaw, M. T., Parnas, R. S., and McDonnell, A.-M. (2006). Investigation of basalt fiber composite mechanical properties for applications in transportation. *Polymer composites*, 27(1):41–48.

[41] Ma, P. C., Kim, J.-K., and Tang, B. Z. (2006). Coating carbon nanotubes with silver nanoparticles to get conductive nanocomposites. In *Electronic Materials and Packaging, 2006. EMAP 2006. International Conference on*, pages 1–4. IEEE.

[42] MAFIC (2018). Basalt continuous fibers. http://www.maficbasalt.com/blog/wp-content/uploads/2016/06/Mafic-Assembled-Roving-TDS-1.pdf. Accessed: 2018-04-01.

[43] Malherbe, S. and Cloete, T. E. (2002). Lignocellulose biodegradation: fundamentals and applications. *Reviews in Environmental Science and Biotechnology*, 1(2):105–114.

[44] Mannan, S., Knox, J. P., and Basu, S. (2017). Correlations between axial stiffness and microstructure of a species of bamboo. *Royal Society open science*, 4(1):160412.

[45] May, C. (1987). *Epoxy resins: chemistry and technology*. CRC press.

[46] Militky, J. and Kovacic, V. (1996). Ultimate mechanical properties of basalt filaments. *Textile Research Journal*, 66(4):225–229.

[47] Mishra, S., Mohanty, A., Drzal, L., Misra, M., Parija, S., Nayak, S., and Tripathy, S. (2003). Studies on mechanical performance of biofibre/glass reinforced polyester hybrid composites. *Composites Science and Technology*, 63(10):1377–1385.

[48] Mohanty, A. K., Misra, M., and Drzal, L. T. (2005). *Natural fibers, biopolymers, and biocomposites*. CRC press.

[49] National Center for Biotechnology Information (2000). M-phenylenediamine. https://pubchem.ncbi.nlm.nih.gov/compound/7935. Accessed: 2018-03-30.

[50] Parameswaran, N. and Liese, W. (1976). On the fine structure of bamboo fibres. *Wood Science and Technology*, 10(4):231–246.

[51] Park, J.-M., Shin, W.-G., and Yoon, D.-J. (1999). A study of interfacial aspects of epoxy-based composites reinforced with dual basalt and sic fibres by means of the fragmentation and acoustic emission techniques. *Composites Science and Technology*, 59(3):355–370.

[52] Ray, D., Sarkar, B. K., Rana, A., and Bose, N. R. (2001). The mechanical properties of vinylester resin matrix composites reinforced with alkali-treated jute fibres. *Composites Part A: applied science and manufacturing*, 32(1):119–127.

[53] Resource Fiber LLC (2018). Bamboo products. http://www.resource-fiber.com/why-bamboo. Accessed: 2018-04-01.

[54] Rich, M., Drzal, L., Hunston, D., Holmes, G., and McDonough, W. (2002). Round robin assessment of the single fiber fragmentation test. In *Procedings of the American Society for Composites 17th Technical Conference*.

[55] Santulli, C. (2004). Critical length measurements in carbon fibers during single fiber fragmentation tests using acoustic emission. *Journal of materials science*, 39(8):2905–2907.

[56] Schneider, C. A., Rasband, W. S., and Eliceiri, K. W. (2012). Nih image to imagej: 25 years of image analysis. *Nature methods*, 9(7):671.

[57] Sella Kapu, N. and Trajano, H. L. (2014). Review of hemicellulose hydrolysis in softwoods and bamboo. *Biofuels, Bioproducts and Biorefining*, 8(6):857–870.

[58] Shao, S., Jin, Z., Wen, G., and Iiyama, K. (2009). Thermo characteristics of steam-exploded bamboo (phyllostachys pubescens) lignin. *Wood science and technology*, 43(7-8):643–652.

[59] Sigma-Aldrich (2000). m-phenylenediamine p23954. https://www.sigmaaldrich.com/catalog/product/aldrich/p23954?lang=en&region=US. Accessed: 2018-03-30.

[60] Singh, S., Simmons, B. A., and Vogel, K. P. (2009). Visualization of biomass solubilization and cellulose regeneration during ionic liquid pretreatment of switchgrass. *Biotechnology and Bioengineering*, 104(1):68–75.

[61] Singha, K. (2012). A short review on basalt fiber. *International Journal of Textile Science*, 1(4):19–28.

[62] Sreekala, M., George, J., Kumaran, M., and Thomas, S. (2002). The mechanical performance of hybrid phenol-formaldehyde-based composites reinforced with glass and oil palm fibres. *Composites science and technology*, 62(3):339–353.

[63] Standard, ASTM (2010). D790 (2010) standard test methods for flexural properties of unreinforced and reinforced plastics and electrical insulating materials. *ASTM International, West Conshohocken*.

[64] Subramanian, R. and Austin, H. (1980). Silane coupling agents in basalt-reinforced polyester composites. *International Journal of Adhesion and Adhesives*, 1(1):50–54.

[65] Thwe, M. M. and Liao, K. (2003). Durability of bamboo-glass fiber reinforced polymer matrix hybrid composites. *Composites science and technology*, 63(3-4):375–387.

[66] Tokoro, R., Vu, D. M., Okubo, K., Tanaka, T., Fujii, T., and Fujiura, T. (2008). How to improve mechanical properties of polylactic acid with bamboo fibers. *Journal of materials science*, 43(2):775–787.

[67] Wade, L. G. (2011). Epoxide. https://www.britannica.com/science/epoxide. Accessed: 2018-03-30.

[68] Wei, B., Cao, H., and Song, S. (2011). Surface modification and characterization of basalt fibers with hybrid sizings. *Composites Part A: Applied Science and Manufacturing*, 42(1):22–29.

[69] Yeasmin, L., Ali, M. N., Gantait, S., and Chakraborty, S. (2015). Bamboo: an overview on its genetic diversity and characterization. *3 Biotech*, 5(1):1–11.

[70] Youssefian, S. and Rahbar, N. (2015). Molecular origin of strength and stiffness in bamboo fibrils. *Scientific reports*, 5:11116.

[71] Zhang, J., Feng, L., Wang, D., Zhang, R., Liu, G., and Cheng, G. (2014). Thermogravimetric analysis of lignocellulosic biomass with ionic liquid pretreatment. *Bioresource technology*, 153:379–382.